# Development of a Robotic Ultrasound System to Assist Ultrasound Examinators

**Maria Bamaarouf, Flavien Paccot, Hélène Chanal, Laurent Sarry**

*Universite Clermont Auvergne INP CNRS Institut Pascal*

Ecole Doctorale Sciences Pour l'Ingénieur

## Research question

Medical ultrasound exams often require that ultrasound technicians hold the transducers in awkward positions for prolonged periods of time, sometimes exerting large forces. This un-ergonomic examination process may lead to work-related musculoskeletal disorders[1], [2].

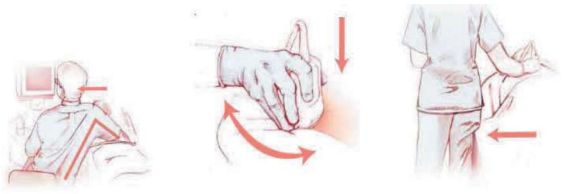

Robotic ultrasound might overcome ultrasound disadvantages through collaborative assistance or even an autonomous system for example :

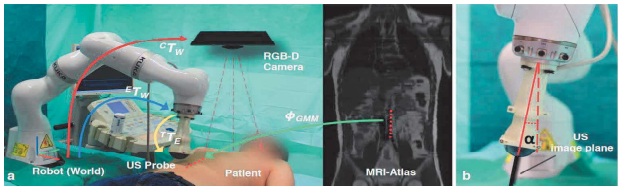


*Example of robotic ultrasound system[3]*

## Materials & Methods

This application uses a 6-axis industrial robot TX2-60. The collaborative robot is equipped with a 6-axis external force/torque Schunk FTN GAMMA 65-5 sensor, an ergonomic handle (probe), and a silicone fake pregnant belly.

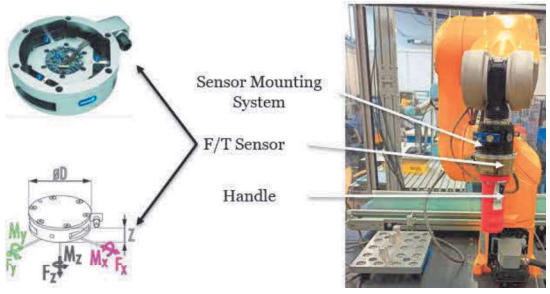


Medical robotic ultrasound sets special safety requirements. In this application, it's ensured through :

- Robot controller
- Inherent safety features of the robot (limited speed, effort, position….
- On/Off buttons to allow the movem

The sensor measures the operator's applied force and the contact force between the probe and the patient skin. The external forces are translated into robot motion. The trajectory generation manages speed and acceleration thresholds as required by the operator which guarantees a safe work environment. The robot trajectory is computed by applying Newton's second law to a virtual solid.

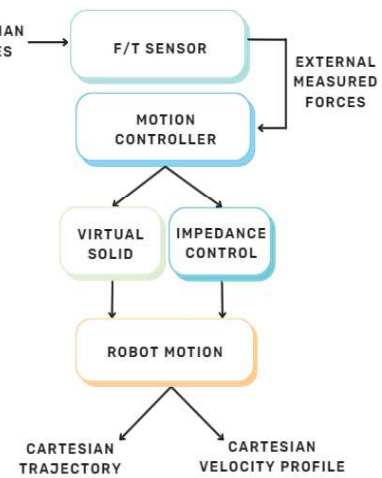


## Objective of the thesis

- **Ensure the co-manipulation in contact with the abdominal wall using a virtual solid.**
- **Use ultrasound images to improve diagnosis with visual servoing.**

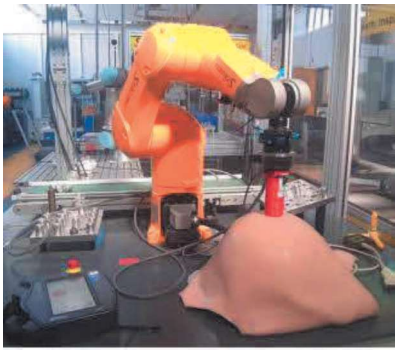

## Digital environment

- To study the robot's behavior when manually guided by the virtual solid method, the trajectory generation law is implemented under Simulink.
- The control strategy is implemented in VAL3 language on the CS9 controller on Stäubli Robotics Suite (SRS).

*Matlab environment*

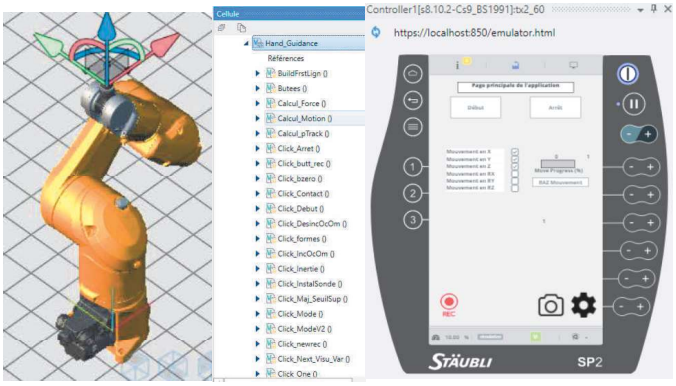


*SRS environment*

## Conclusion

**A new co-manipulation control strategy is developed based on the path computation of a virtual solid under the operator's interaction. Compared to classical impedance control, parameter adjustment is easier and the required operator forces are lighter, which reduces musculoskeletal disorders.**

## Bibliography

1. G. Harrison et A. Harris, « Work-related musculoskeletal disorders in ultrasound: Can you reduce risk? », *Ultrasound*, vol. 23, nº 4, p. 224-230, nov. 2015, doi: 10.1177/1742271X15593575.
2. K. Evans, S. Roll, et J. Baker, « Work-Related Musculoskeletal Disorders (WRMSD) Among Registered Diagnostic Medical Sonographers and Vascular Technologists: A Representative Sample », *J. Diagn. Med. Sonogr.*, vol. 25, nº 6, p. 287-299, nov. 2009, doi: 10.1177/8756479309351748.
3. S. Virga et al., « Automatic force-compliant robotic ultrasound screening of abdominal aortic aneurysms », in 2016 IEEE/RSJ International Conference on Intelligent Robots and Systems (IROS), Daejeon, South Korea: IEEE, oct. 2016, p. 508-513. doi: 10.1109/IROS.2016.7759101.

# Calcul de trajectoire de robot pour la fabrication additive de tubulures complexes

Directrice de thèse : Hélène CHANAL – Co directeur de thèse : Emmanuel DUC

**Antoine BACCOMO**

Thèse financée par la Région Auvergne-Rhône-Alpes, projet CraFT

## Contexte et problématique

- Fabrication d'une pièce mono cordon grâce au procédé WAAM couplé au procédé CMT

- Appariation de discontinuités sur le cordon de dépose au niveau des changements de direction

## Objectifs

Développer une méthode rapide d'estimation de l'accélération et du jerk de la torche, en fonction de la vitesse, en vue de définir les zones critiques

Développer un processus de calcul de trajectoires d'un robot de fabrication additive pour les pièces complexes de type tubulure.

## Procédé de fabrication WAAM

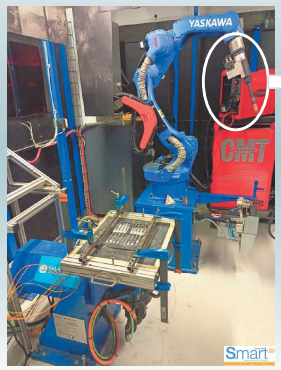


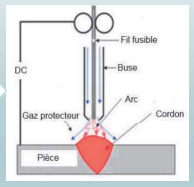


Procédé CMT

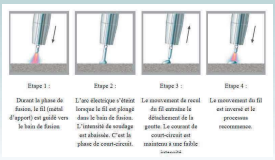

## Chaine numérique de la fabrication additive

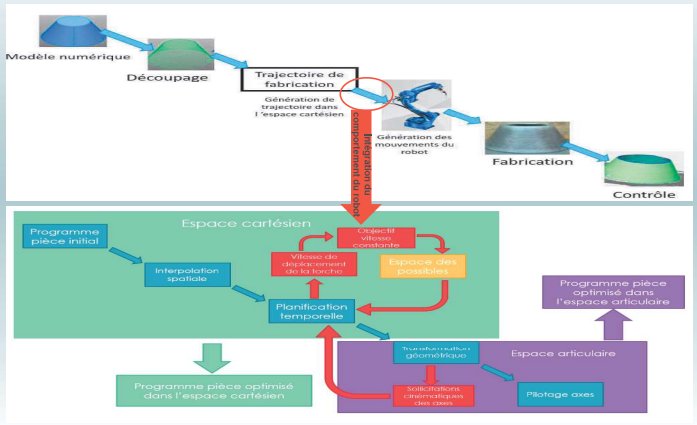


## Estimation de l'accélération et du jerk

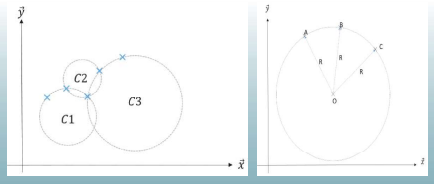


Méthode d'interpolation par trois points

Déduction du rayon

R

$$\|\vec{\Gamma}\| = \frac{d^2 s}{dt^2} = \frac{Vc^2}{R}$$

$$\|\vec{J}\| = \frac{d^3 s}{dt^3} = \frac{Vc^3}{R^2}$$

Recherche des zones critiques

## Validation de la méthode

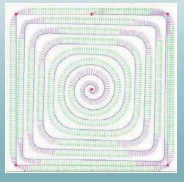

Résultats attendus

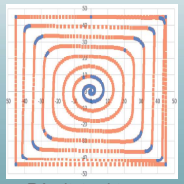

Résultats obtenus

Résultats non conformes aux attentes

La vitesse ne varie pas instantanément

Nécessité de prendre en compte les zones tampons avant et après les virages

## Détermination de la vitesse de la torche

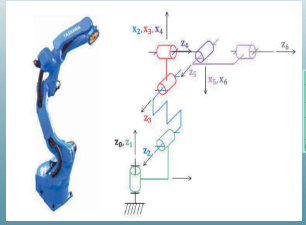

Modélisation du robot

Détermination des paramètres cinématiques du robot (Méthode de Denavit-Hartenberg)

Modèle géométrique direct

Modèle géométrique indirect

Modèle cinématique direct

Détermination des paramètres cinématiques du robot

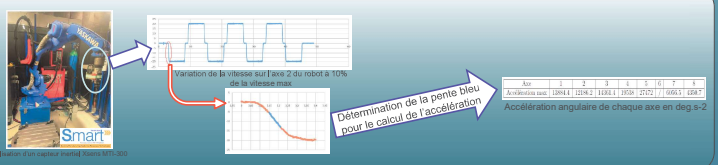


## Bibliographie

[Pateloup, 2005] Pateloup, V. (2005). *Amélioration du comportement cinématique des machines outils UGV*. PhD thesis, Université Blaise Pascal-Clermont-Ferrand II.

[Querard, 2019] Querard, V. (2019). *Réalisation de pièces aéronautiques de grandes dimensions par fabrication additive WAAM*. PhD thesis, École centrale de Nantes.

[Chalvin et al., 2020] Chalvin, M., Campocasso, S., Hugel, V., and Baizeau, T. (2020). Layer-by-layer generation of optimized joint trajectory for multi-axis robotized additive manufacturing of parts of revolution. *Robotics and Computer-Integrated Manufacturing*

# Poutres mixtes acier-béton avec connecteurs démontables pour le réemploi

Lina BASSIL, Sébastien DURIF, Abdelhamid BOUCHAIR, Khaled EL-TAWIL
*Université Clermont Auvergne, Université Libanaise*

Ecole doctorale Sciences Pour l'Ingénieur

INSTITUT PASCAL sciences de l'ingénierie et des systèmes

## Introduction

Poutres mixtes acier-béton : les connexions sont des clefs à maîtriser

X. Chen et al., Shear behavior of large studs and novel bolted connectors in steel-UHPC composite beams, Structures 45 (2022) 2091–2103

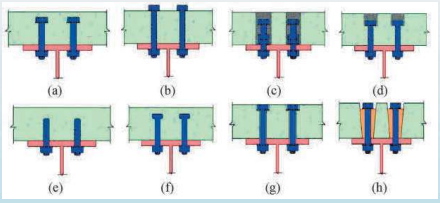


L. Xiong et al., Demountable connections for enhanced resilience: An analytical and numerical assessment of steel-concrete composite beams , Journal of Building Engineering 70 (2023) 106392

**Connecteurs soudés**

Connecteurs courants : goujons à tête noyés dans le béton et soudés à l'acier

- Couverts par les normes actuelles et leurs méthodes de calcul
- Faciles à installer en ateliers équipés
- Difficilement démontables pour la déconstruction et/ou le réemploi

**Connecteurs démontables**

En cours de développement : boulons ou systèmes équivalents

- Démontabilité et réemploi possibles : poutre acier et dalle béton
- Utilisation en réhabilitation de l'existant (même le non soudable)
- Réponse aux attentes : bilan carbone et développement durable

## Objectifs

- Maîtrise du comportement des connecteurs démontables et comparaison avec les soudés.
- Développement de modèles MEF 3D pour avoir des outils performants.
- Analyse des lois force-glissement : rigidité initiale, résistance, ductilité, mode de ruine.
- Identification des formes et matériaux adéquats pour un maximum d'efficacité des connexions.
- Proposition de formules analytiques pour déterminer la résistance et la rigidité des connexions démontables.
- Évaluation de l'impact (ELS et ELU) de connecteurs démontables dans des poutres de planchers.

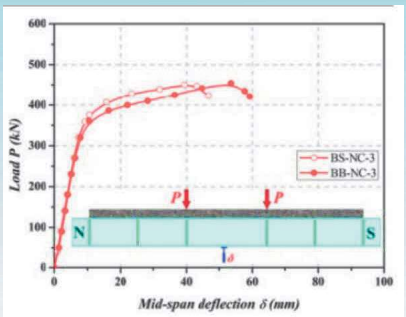


*Résultat d'essai push-out comparant connecteurs soudé (BS) et boulonné (BB)*

Z. Fang et al., Interfacial shear and flexural performances of steel–precast UHPC composite beams: Full-depth slabs with studs vs. demountable slabs with bolt, Engineering Structures Volume 260, 1 June 2022, 11423.

## Méthodes

- **Développement** de modèles **MEF 3D** tenant compte de l'**endommagement** du béton et du comportement réel de l'acier (logiciel ATENA).
- **Validation** des modèles par comparaison aux essais existants
- Réalisation d'un **programme expérimental**
  - push-out : loi élémentaire force-glissement
  - flexion : loi de comportement de poutres de différentes configurations
- Etude paramétrique sur différentes configurations de connecteurs :
  - Evaluation de l'applicabilité des formules analytiques existantes aux connecteurs démontables
  - Proposition de formes spécifiques de connecteurs et leurs formules analytiques de calcul

$$P_{Rd1} = \frac{0.8\, f_u\, \pi\, d^2/4}{\gamma_V} \qquad P_{Rd2} = \frac{0.29\, \alpha\, d^2 \sqrt{f_{ck} E_{cm}}}{\gamma_V}$$

*Formules de calcul de la résistance des connecteurs soudés selon l'Eurocode 4.*

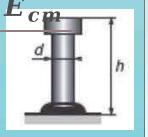


## Résultats

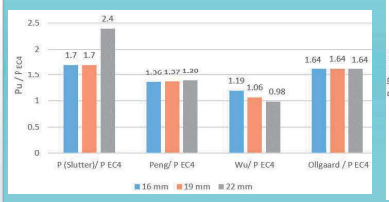


*Rapport entre la résistance analytique des références [1],[2],[3] et [4] et celle de l'Eurocode 4 (cisaillement des connecteurs soudés)*

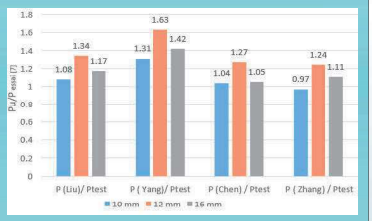


*Rapport entre la résistance analytique des références [5],[6],[7] et [8] et les essais de la référence [7] (cisaillement des connecteurs démontables)*

*Maillage d'un essai push-out avec 4 connecteurs soudés et loi force-glissement (logiciel ATENA)*

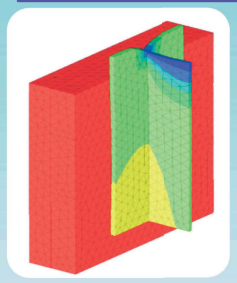

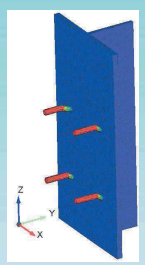


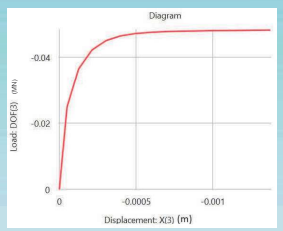


## Conclusion

1. Connecteurs soudés : les formules analytiques existantes évaluent correctement la résistance.
2. Connecteurs démontables :
   - Absence de formules analytiques dans les règlements de construction
   - Formules proposées par différents auteurs : à évaluer par essais et MEF
3. Modèle MEF développé sous ATENA : résultats prometteurs pour représenter le comportement réel des connecteurs soudés et boulonnés.

## Références

1. Slutter R. G., Driscoll G. C., Flexural Strength of Steel-Concrete Composite Beams, J. Struct. Div., 1965, vol.91, n°2, pp.71-99.
2. Ollgaard J.G., Slutter R.G., Fisher J.W., Shear strength of stud connectors in lightweight and normal-density concrete, AISC Engineering Journal, 1971, vol. 8, n°2, pp. 55-64.
3. Peng, K.; Liu, L.; Wu, F.; Wang, R.; Lei, S.; Zhang, X. Experimental and Numerical Analyses of Stud Shear Connectors in Steel–SFRCC Composite Beams. Materials 2022, 15, 4665.
4. Wu, F.; Tang, W.; Xue, C.; Sun, G.; Feng, Y.; Zhang, H. Experimental Investigation on the Static Performance of Stud Connectors in Steel-HSFRC Composite Beams. Materials 2021, 14, 2744.
5. Xinpei Liu; Mark A. Bradford, Dist.M.ASCE; and Michael S. S. Lee Behavior of High-Strength Friction-Grip Bolted Shear Connectors in Sustainable Composite Beams Journal of Structural Engineering July 24, 2014, ISSN 0733-9445/04014149
6. Fei Yang, Yuqing Liu*, Zhibo Jiang, Haohui Xin Shear performance of a novel demountable steel-concrete bolted connector under static push-out tests Engineering Structures 160 (2018) 133–146
7. Jun Chen, Wei Wang, Fa-xing Ding, Ping Xiang Behavior of an Advanced Bolted Shear Connector in Prefabricated Steel-Concrete Composite Beams, Materials 12 september 2019
8. Zhang, Y.J.; Liu, A.; Chen, B.C.; Zhang, J.P.; Pi, Y.; Bradford, M.A. Experimental and numerical study of shear connection in composite beams of steel and steel-fibre reinforced concrete. Eng. Struct. 2020, 215, 110707
9. EN 1994-1-1, Eurocode 4 (2004 Calcul des structures mixtes acier-béton– Partie 1-1: Règles générales et règles pour les bâtiments, Comité européen de normalisation (CEN), Bruxelles.

# Network Path Validation for Packets Delivery

Dorine CHAGNON dorine.chagnon@doctorant.uca.fr
Kévin THIRY-ATIGHEHCHI kevin.atighehchi@uca.fr
Gérard CHALHOUB gerard.chalhoub@uca.fr
Université Clermont Auvergne, CNRS, Mines Saint-Etienne, LIMOS, France

## Objectives

1. Motivate the path validation.
2. Expose the problems around path validation.
3. Expose a state-of-the-art of path validation protocols.

## Introduction

- In the current Internet, routers have full control over packet delivery.
- Current Internet supports neither enforcement nor verification of packet path.
- Path validation enables end-hosts to enforce the path for their transmissions.
- Path validation allows a node to verify that the packet followed an approved path.

## Examples of Needs

- A company might want to control through which providers its traffic is forwarded between its branches.
- A recipient might request that packets pass through an intrusion detection service before their arrival.

## Desired Properties for Path Validation

- **Path enforcement** assures a packet is forwarded on the agreed path over each en-route node in the correct order.
- **Path verification** assures that the sender, the intermediate, and the destination routers are able to verify that the forwarded packet has followed the correct path.

## Attacks Overview

- **Skipping attack**:

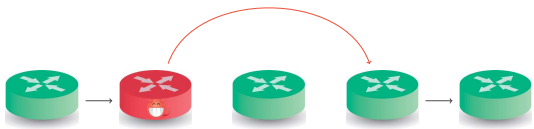

- **Out-of-order attack**:

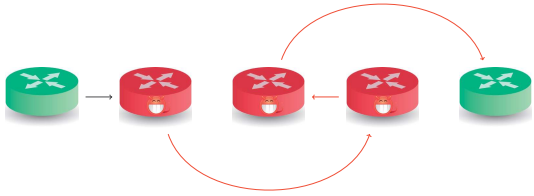

- **Addition attack**:

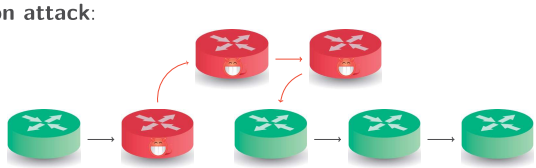

- **Detour attack**:

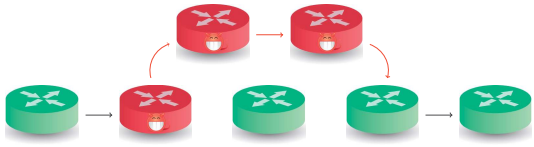

## Before Path Validation Protocols

| Solution | Goal | Limitation |
|---|---|---|
| Secure routing | Securely find the best paths connecting end-hosts | The packet delivery does not have to follow this best path |
| Secure source routing | Path enforcement | Inefficient together |
| Secure traceroute | Path verification | |

## Steps of Path Validation [1]

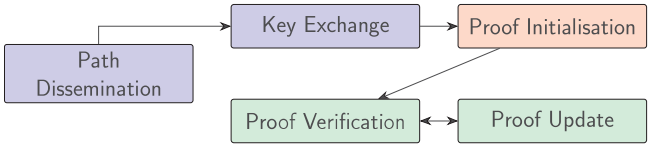


## State-of-the-art

- **ICING** builds a verifier for each router. The cryptographic proof of the current router is the result of the xor aggregation of the proofs shared with each of the current predecessors of the router.
- **OPT** (Origin and Path Trace) builds the proof assuming the source is trusted. A general verifier allows en-route router to verify their personal verifier before updating this general verifier used by the next hop.
- **OSV** (Orthogonal Sequence Verification) is similar to OPT except that instead of using cryptographic proof, it uses orthogonal sequences and does inner product.
- **PPV** uses a flow of packets to validate a path. A router marks a packet with a certain probability. The gathering of all the marks from all the packets enables the validation of the forwarding process.
- **Atomos** [2] uses asymmetric cryptographic proofs and only one verifier that aggregates the proof of all the routers.
- **PrivNPV** [3] (Privacy-preserving network path validation) hides the path from routers and their position on this path.
- **EPIC** [4] (Every Packet Is Checked) uses shorter verification fields while maintaining the same level of security thanks to timestamps.

## References

[1] Kai Bu, Avery Laird, Yutian Yang, Linfeng Cheng, Jiaqing Luo, Yingjiu Li, and Kui Ren. Unveiling the Mystery of Internet Packet Forwarding: A Survey of Network Path Validation *ACM Comput. Surv.*, 53(5):104:1–104:34, September 2020.

[2] Anxiao He, Kai Bu, Yucong Li, Eikoh Chida, Qianping Gu, and Kui Ren. Atomos: Constant-Size Path Validation Proof. *IEEE Transactions on Information Forensics and Security*, 15:3832–3847, 2020. Conference Name: IEEE Transactions on Information Forensics and Security.

[3] Binanda Sengupta, Yingjiu Li, Kai Bu, and Robert H. Deng. Privacy-preserving Network Path Validation. *ACM Trans. Internet Technol.*, 20(1):5:1–5:27, February 2020.

[4] Markus Legner, Tobias Klenze, Marc Wyss, Christoph Sprenger, and Adrian Perrig. EPIC: every packet is checked in the data plane of a path-aware internet. In *Proceedings of the 29th USENIX Conference on Security Symposium*, SEC'20, pages 541–558, USA, August 2020. USENIX Association.

## Acknowledgments

- The authors acknowledge the support of the Chaire de confiance numérique (12LIMO11LIMOS on FCA)

# Algorithmics and Structure of Identification Problems

Dipayan CHAKRABORTY (2nd year PhD), Annegret WAGLER (Director of Thesis) and Florent FOUCAUD (Co-Supervisor)

LIMOS, Université Clermont Auvergne

## Introduction

- Fault analysis in multiprocessor networks, detection of intruders and threats in facilities and many other such practical necessitites have over the years given rise to a particular genre of problems in graphs called the *identification problems*. In this genre, given a graph $G = (V, E)$, the objective is to uniquely identify each vertex of a subset $S$ of $V$ ($S = V$ for example, for the majority of problems in the literature). To that end, the most common tool used is to associate a unique *codeword* with each vertex of $G$ and then identify the vertices by means of their codewords. In the literature is usually done the following way:
  - Introduce a discrete set $X$ (usually either a dominating set (DS) or a total-dominating set (TDS) of $G$).
  - With each $u \in S$, associate the *codeword* $X(u)$, where $X(u)$ is usually either $N_G(u) \cap X$ or $N_G[u] \cap X$ in the literature.
  - Require that for all distinct $u, v \in S$, we must have $X(u) \neq X(v)$.

  Then $X$ is called a *code* of $G$. Table 1 gives examples of some of the more well-studied types of identification problems in the literature.

## Table 1

| Problem Name | $X$ | $X(u)$ | $S$ | $\min \lvert X\rvert$ |
|---|---|---|---|---|
| Identifying Codes (IDC) | Dominating Set | $N_G[u] \cap X$ | $V$ | $\gamma_{ID}(G)$ |
| Locating-Dominating Codes (LDC) | Dominating Set | $N_G(u) \cap X$ | $V - X$ | $\gamma_{LD}(G)$ |
| Locating-Total Dominating Codes (LTDC) | Total Dominating Set | $N_G(u) \cap X$ | $V - X$ | $\gamma_{LTD}(G)$ |
| Open Locating-Dominating Codes (OLDC) | Total Dominating Set | $N_G(u) \cap X$ | $V$ | $\gamma_{OLD}(G)$ |
| Neighbour-Locating Colouring (NCol) | $\mathscr{X}$ proper $k$-colouring; $X = \{0, 1, \ldots, k-1\}$ | $(\mathscr{X}(u), \{\mathscr{X}(v) : v \in N_G(u)\})$ | $V$ | $\chi_{NCol}(G)$ |
| Locating Colouring (LCol) | $\mathscr{X}$ proper $k$-colouring; $X$ = set of colour classes | $((d_G(u, X_i)))$ | $V$ | $\chi_{LCol}(G)$ |

Table 1: Examples of some of the more well-studied identification problems in graphs

## Interesting Questions Explored

1. What are the bounds on the cardinalities of the minimum-ordered codes (the parameters $\gamma_{\text{problem name}}(G)$ for example in Table 1) of a graph $G$ with respect to a particular problem?
2. Is there a characterization of the extremal graphs for which $|X| = |V|$ or $|V| - 1$, for example?
3. What are the computational complexitites of the corresponding decision problems to find a minimum-ordered code of $G$ in general or when $G$ belongs to a special graph class?

## Work on block graphs

- **New bounds and constructions for neighbor-locating colorings of graphs**. [1]
  - In this work, we address the problems of IDC, LDC and OLDC (refer to Table 1) on block graphs (diamond-free chordal graphs).
  - We find tight bounds on the parameters $\gamma_{ID}(G)$, $\gamma_{LD}(G)$ and $\gamma_{OLD}(G)$, respectively.
  - In the process, we also prove for block graphs the following two conjectures from the literature.
    - [2] when $G$ is a block graph, $\gamma_{ID}(G)$ is at most the number of *blocks* (maximal cliques).
    - [3] $\gamma_{LD}(G) \leq \frac{|V|}{2}$ for graphs $G$ without isolated vertices.

## Work on Neighbour-Locating Colouring (NLCol)

- **New bounds and constructions for neighbor-locating colorings of graphs** [4]
  - In this article, we look at identification problems through the lens of graph colourings and compare on general graphs the parameters $\chi(G)$ (the usual chromatic number of graph colourings), $\chi_{LCol}(G)$ and $\chi_{NLCol}(G)$ (refer to Table 1).
  - In particular, for any three positive integers $p, q, r$ with $2 \leq p \leq q \leq r$ (except for $2 = p = q < r$), we construct connected graphs $G_{p,q,r}$ with $\chi(G_{p,q,r}) = p$, $\chi_{LCol}(G_{p,q,r}) = q$ and $\chi_{NLCol}(G_{p,q,r}) = r$.
  - We also look at NLCol on sparse graphs $G$ with $|E| \leq a|V| + b$ and $\chi_{NLCol}(G) = k$. For such graphs, we find an upper bound of order $O(k^{2a+1})$ on $|V|$; and provide constructions of sparse graphs whose orders nearly reach the upper bound.
  - We also prove that the corresponding decision problem to find an NL-colouring of a sparse graph with $k$ colours is NP-Complete.

## Work on Locating-Total Dominating Codes (LTDC)

- **Progress towards the two-thirds conjecture on locating-total-dominating sets** [5]
  - In this work, we inspect an existing two-thirds conjecture [6] on the problems of LTDC (refer to Table 1) which says that for a twin-free and isolate-free graph $G$, we have $\gamma_{LTD}(G) \leq \frac{2}{3}|V|$.
  - We provide significant confirmation to the conjecture by proving it to be true on a variety of graph classes, namely, Cobipartite graphs, Split graphs, Block graphs, Subcubic graphs and Outerplanar graphs.

## Conclusion

- In the thesis, we prove for some graph classes some of the more important and interesting conjectures from the literature.
- We have also looked at newer problems (of NLCol and LCol) in the genre where the identification happens by means other than by classical (total) dominating sets.
- We have compared the different versions of the identification problems on certain graph classes thus providing a clearer picture of the problem genre.

## References

[1] Dipayan Chakraborty, Florent Foucaud, Aline Parreau, and Annegret Katrin Wagler. On three domination-based identification problems in block graphs. In *Algorithms and Discrete Applied Mathematics - 9th International Conference, CALDAM 2023, Gandhinagar, India, February 9-11, 2023, Proceedings*, volume 13947 of *Lecture Notes in Computer Science*, pages 271–283. Springer, 2023.

[2] Gabriela R. Argiroffo, Silvia M. Bianchi, Yanina Lucarini, and Annegret K. Wagler. On the identifying code number of block graphs. In *Proceedings of ICGT 2018, Lyon, France*, 2018.

[3] Delia Garijo, Antonio González, and Alberto Márquez. The difference between the metric dimension and the determining number of a graph. *Applied Mathematics and Computation*, 249:487–501, 2014.

[4] Dipayan Chakraborty, Florent Foucaud, Soumen Nandi, Sagnik Sen, and D. K. Supraja. New bounds and constructions for neighbor-locating colorings of graphs. In *Algorithms and Discrete Applied Mathematics - 9th International Conference, CALDAM 2023, Gandhinagar, India, February 9-11, 2023, Proceedings*, volume 13947 of *Lecture Notes in Computer Science*, pages 121–133. Springer, 2023.

[5] Dipayan Chakraborty, Florent Foucaud, Anni Hakanen, Michael A. Henning, and Annegret Wagler. Progress towards the two-thirds conjecture on locating-total dominating sets. *CoRR*, abs/2211.14178, 2022.

[6] Florent Foucaud and Michael A Henning. Locating-total dominating sets in twin-free graphs: a conjecture. *The Electronic Journal of Combinatorics*, 23.

## Contact Information

- Web: https://dipayan5186.github.io/Website/
- Email: dipayan.chakraborty@uca.fr

Journées Scientifiques des Doctorants SPI 2023
Ecole Doctorale des Sciences Pour l'Ingénieur

# Nanofibres de cellulose pour l'isolation thermique de panneau sandwich

CHIN Yi Hien[1,2], BIWOLE Pascal[1,3], GRIL Joseph[1,4], MOUTOU PITTI Rostand[1,5], VIAL Christophe[1], OULDBOUKHITINE Salah-Eddine[1], GURCEL Benjamin[2], LABONNE Nicolas[2]

[1]Université Clermont Auvergne, CNRS, SIGMA Clermont, Institut Pascal, 63000 Clermont Ferrand, France.
[2]Société Dagard, 23600 Boussac, France.
[3]Mines Paris, Université PSL, Centre Procédés Energies Renouvelables et Systèmes Energétiques (PERSEE), 06904 Sophia Antipolis, France
[4]Université Clermont Auvergne, INRAE, PIAF, 63000 Clermont Ferrand, France.
[5]CENAREST, IRT, BP 14070, Libreville, Gabon.
*yi_hien.chin@uca.fr*

## Contexte et objectif

Le panneau sandwich est un élément de construction modulaire composé d'une âme isolante et de parements sur ses deux faces. Il est nécessaire d'élaborer un matériau biosourcé capable de se substituer aux isolants actuels issus de la pétrochimie. Nous cherchons à **augmenter la porosité de bois par délignification** afin de **réduire sa conductivité thermique** en conservant la structure hiérarchique. L'objectif de la thèse consiste à concevoir un panneau sandwich avec une âme en bois délignifié isolant.

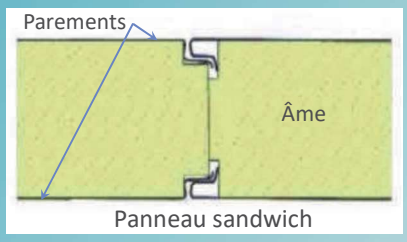


## Méthodes

Fabrication de nouvel isolant à base de nanofibres de cellulose:

**Délignification** → Procédé existant en papeterie → **Séchage industrialisable** → Préserver la porosité créée

Méthodologie expérimentale:


Analyse par spectroscopie infrarouge à transformée de Fourier
→ Détecter la présence de lignine


Détermination de la surface spécifique par sorption d'azote
→ Confirmer la création d'une nouvelle porosité


Observations morphologique (MEB, tomographie X)
→ Estimer le flux thermique par modélisation multi-échelle


Détermination de conductivité thermique
→ Vérifier le caractère isolant thermique


Mesure de sorption d'eau
→ Identifier les propriétés de transfert d'humidité


Essais de compression, traction et cisaillement
→ Vérifier la compatibilité pour l'usage en cloison

Analyse de cycle de vie

- Qualifier l'usure et la fatigue
- Quantifier la durée de vie
- Quantifier les émissions de $CO_2$ et la consommation énergétique du bâtiment
- Pistes de recyclage ou revalorisation en fin de vie

Procédé de fabrication optimisé en vue d'une industrialisation

- Recherche d'un degré de délignification optimal
- Analyse des coûts

## Résultats

Résultats obtenus:

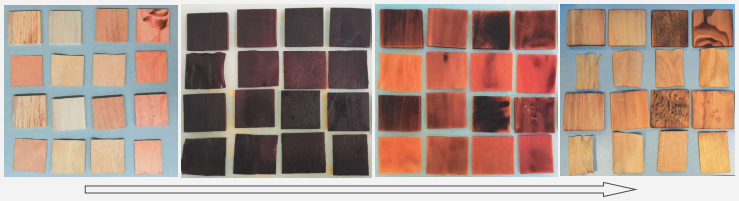

*Variation de couleur et de dimension des bois aux différents stades de délignification. 1ère colonne à 4e colonne: Hêtre, Peuplier, Chêne, Douglas. 1ère et 3e ligne: bois massif d'1 cm d'épaisseur. 2e et 4e ligne: placages de bois.*

- Le traitement par **délignification** permet de **réduire la masse** et la conductivité thermique [1]
- Le **retrait dû au séchage** pourrait augmenter la densité à cause de l'effondrement de cellules
- Parmi les essences françaises, le **peuplier** peut potentiellement atteindre une conductivité thermique suffisamment faible après une modification adéquate

Résultats attendus:

- Conductivité thermique < 0,042 W/m.K
- Meilleure résistance aux sollicitations mécaniques que le matériau d'âme actuel
- Modèles permettant de prédire le flux thermique et la rentabilité économique

## Conclusions et Perspectives

- Afin de réduire davantage la conductivité thermique, il faut **augmenter le degré de délignification** et **réduire la déformation lors du séchage**.
- Pour compléter la caractérisation, une **étude théorique des transferts thermiques** à l'échelle paroi cellulaire, panneau sandwich et locaux sera menée.
- En complément, il serait intéressant d'étudier le **comportement au feu**, la **résistance aux moisissures**, la **performance acoustique** et la **biodégradabilité** pour ce nouveau matériau à base de nanofibres de cellulose.

**Remerciements**

Les auteurs remercient l'Agence Nationale de la Recherche (ANR) et la société Dagard pour le financement de la thèse via le plan « France Relance »

**Bibliographie**

[1] T. Li, J. Song, X. Zhao, *et al.*, Anisotropic, lightweight, strong, and super thermally insulating nanowood with naturally aligned nanocellulose. Sci. Adv. 4, eaar3724 (2018)

# Knowledge-Based Explainability for Deep Neural Networks

Rim El Cheikh, Issam Falih, Engelbert Mephu Nguifo

Université Clermont Auvergne, Clermont Auvergne INP, ENSMSE, CNRS, LIMOS, F-63000 Clermont–Ferrand, France

## Context

Deep neural networks (DNN) are systems that allow a machine, by means of mathematical functions and optimization algorithms, to learn a specific task. For example, predicting a medical diagnosis with very good accuracy. The process followed by a DNN to give a decision is very complex and incomprehensible for a human user. The purpose of **explainability** is to give some degree of transparency to the path taken by the DNN to arrive at a certain decision, so as to make its process more reliable and its decision convincing to the user.

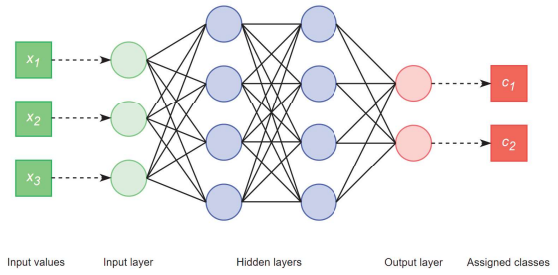


Figure 1:Multi-Layered Perceptron

## Objectives

- The main objective is to develop an explainability method for neural networks that integrate expert knowledge into the decision process in order to make it some intelligible for the user.
- Focus on knowledge introduced at the level of defining the topology of the neural architecture and/or training it.

## Knowledge at the post-hoc level

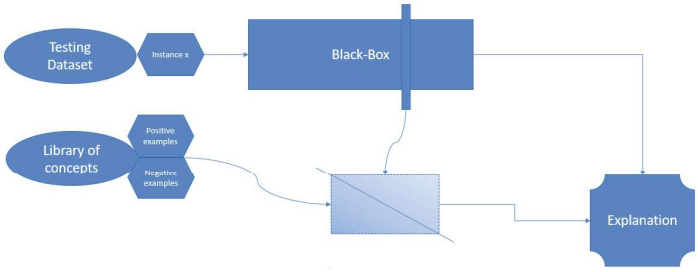


Figure 2:Using the DNN as a Black-Box

- The quality of the model is not taken into account.
- The consistency of an explanation and its alignment with the true inner workings of the underlying model are difficult to verify.

## Knowledge at the training level

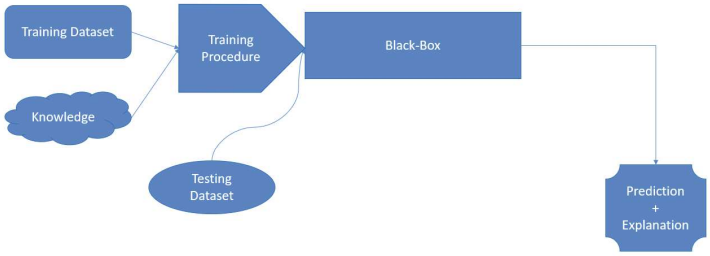


Figure 3:Training the DNN

- Relies on another XAI method for intermediate feature importance scores.
- Explanatory concepts are not labeled.

## Knowledge at the design level

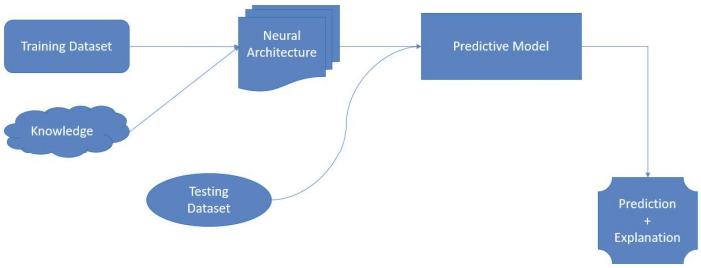


Figure 4:Designing the DNN

## Properties and Characterization

- Explainability approaches are compared based on a set of requirements that allows to check if the properties that the method fulfills correspond to the user's expectations.
  - Scope : Local, Cohort, Global
  - Family : Counterfactual, Abductive, Plausible, Prototypes
  - Completeness : To what extent does the explanation cover the underlying model ?
- Some works aim to formally define and describe an explainability method.

## Perspectives

- Extend characterisation and formalization to cover knowledge-based approaches.
- Design an explainability method so as to:
  - Anticipate explanatory elements based on prior knowledge to make explanations more relevant and aligned with the area in question. In addition, the explanation will be adjusted towards the user's expectations.
  - Provide a prediction as well as its explanation not only faithful to each other but also to the real world.
- Explore the utility of Formal Concept Analysis.

| | | Attributs | | | |
|---|---|---|---|---|---|
| | | Black (a) | White (b) | Blue (c) | Brown (d) |
| Classes | Collie (1) | | x | | x |
| | Walrus (2) | | | | x |
| | Racoon (3) | x | x | | |
| | Cow (4) | x | x | | x |
| | Dolphin (5) | | x | x | |

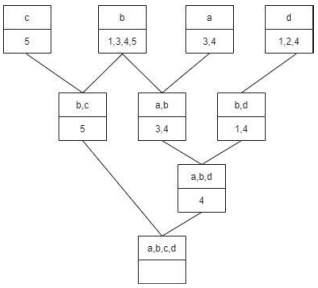


## References

[1] Been Kim et al. Interpretability beyond feature attribution: Quantitative testing with concept activation vectors (tcav). In *International conference on machine learning*, pages 2668–2677. PMLR, 2018.

[2] Natalia Díaz-Rodríguez et al. Explainable neural-symbolic learning (x-nesyl) methodology to fuse deep learning representations with expert knowledge graphs: The monumai cultural heritage use case. *Information Fusion*, 79:58–83, 2022.

[3] Lauraine Tiogning Kueti et al. Using boolean factors for the construction of an artificial neural networks. *International Journal of General Systems*, 47(8):849–868, 2018.

## Acknowledgments

This work benefited from a French government grant managed by the National Research Agency (ANR) under the 'Investissements d'Avenir" program (PIA) with the following reference : ANR-20-SFRI-0003.

# Identifications de Sources de Perturbation Électromagnétique: Applications a des problèmes de CEM.


**B. El Mokhtari, P. Bonnet, G. Al Achkar**

*Université Clermont-Auvergne, Institut Pascal*

Ecole doctorale Sciences Pour l'Ingénieur


## Objectifs

- Étude visant à contrôler les sources de perturbations électromagnétiques dans divers environnements tels que les lignes de transmission et l'espace libre, en analysant les différentes méthodes numérique.

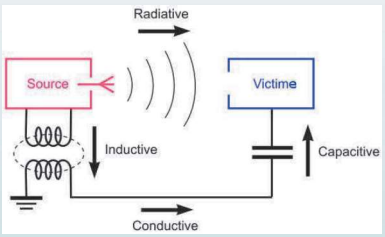


**Type de perturbation**

- Évaluation des limitations des approches existantes, en particulier de la méthode LCCF, pour déterminer leur efficacité dans l'identification des sources de perturbations électromagnétiques.
- Analyse des avantages offerts par les techniques de l'apprentissage automatique (machine learning) et leur application potentielle dans le domaine de l'identification des sources de perturbations électromagnétiques.

## Introduction

- Dans le domaine de la Compatibilité Électromagnétique, l'identification des sources de perturbations électromagnétiques constitue un domaine de recherche vaste. Dans le cadre temporel, il existe quelques méthodes efficaces pour les problèmes linéaires, tandis que dans le domaine fréquentiel, il n'existe pas de méthodes directes précises permettant d'identifier les sources de perturbation. Cela souligne la nécessité de développer des techniques répondant à ces besoins actuels et émergents.

## Méthode LCCF

- On cherche la source $S = (S_d, S_{d+1}, \dots., S_{f-1}, S_f)$ telle que $A.S = C$, avec $C = (C_d, C_{d+1}, \dots., C_{f-1}, C_f)$ représente l'allure du champ cible et $A$ représente la matrice de caractérisations du système électromagnétique étudié.
- Pour construire la matrice $A$ on envoie un signal connu $E = (E_0, E_1, \dots., E_{f-1}, E_f)$ au niveau de l'entrée du système EM et on enregistre la réponse du système au point de contrôle considéré $R = ((R_0, R_1, \dots., R_{f-1}, R_f)$.
- Pour un temps de contrôle $t \in [t_d, t_f]$, la matrice $A$ est donnée par :

$$A = \begin{pmatrix} R_d & R_{d-1} & R_{d-2} & \cdots & R_1 & 0 & \cdots & 0 \\ R_{d+1} & R_d & R_{d-1} & \cdots & R_2 & R_1 & \cdots & 0 \\ R_{d+2} & R_{d+1} & R_d & \cdots & R_3 & R_2 & \cdots & 0 \\ \vdots & \vdots & \vdots & \ddots & \vdots & \vdots & \vdots & \vdots \\ R_f & R_{f-1} & R_{f-2} & \cdots & R_{d+1} & R_d & \cdots & R_1 \end{pmatrix}$$

- La source obtenue par l'application de l'opérateur d'optimalité de Thikonov:

$$S_\beta = \left(\boldsymbol{R^T}.\boldsymbol{R} + \beta.\boldsymbol{I}\right)^{-1}.\boldsymbol{R^T}.C$$

## Résultats

- Intégrité de signal:

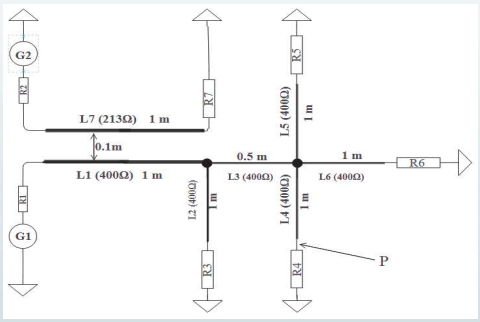


**Système étudié**

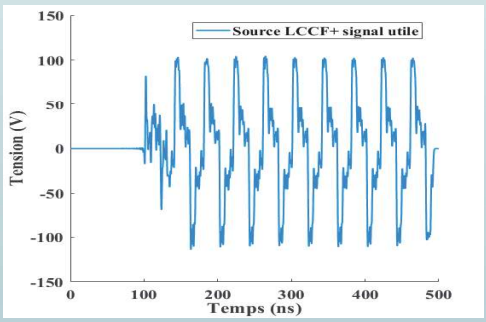


**Signal au niveau de générateur G1**

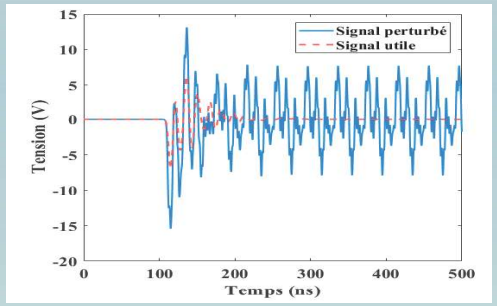


**Signal perturbé et signal utile au niveau du point de control P**

## Conclusion

- Nous avons prouvé que la méthode LCCF est capable d'identifier les sources de perturbations temporelles dans des environnements linéaires.
- L'application de la méthode LCCF a permis de supprimer efficacement la diaphonie dans une ligne de transmission, garantissant ainsi l'intégrité du signal.

## Perspective

- Mise en place d'application expérimentale.
- Application des réseaux de neurone.

## References


1. A. Mori *et al.*, "*Design-oriented EMC analysis of wiring systems*," *2020 International Symposium on Electromagnetic Compatibility - EMC EUROPE*, pp. 1-6, 2020.
2. M. Ali, E. Labouré, and F. Costa, "*Integrated Active Filter for Differential-Mode Noise Suppression*," IEEE Transactions on Power Electronics, vol. 29, no. 3, pp. 1053–1057, 2014.
3. J . Benoit, C. Chauvière, and P. Bonnet, "*Source identification in time domain electromagnetics*," Journal of Computational Physics, vol. 231, no. 8, pp. 3446-3456, 2012



Contact: Brahim.el_mokhtari@uca.fr

# Intensification de la méthanation biologique ex-situ dans un bioréacteur à agitation pneumatique

A.ESSID[1], J.-P. FONTAINE[1], A.-V. URSU[1], C. VIAL[1]

[1]Clermont Auvergne INP, CNRS, Institut Pascal, 63000 Clermont-Fd, France

## Questions scientifiques?

Les niveaux de consommation mondiales en énergie ainsi que la demande qui ne cessent d'augmenter induisent un épuisement progressif des ressources fossiles (pétrole, charbon…) ainsi qu'une augmentation des émissions des gaz à effet de serre ($CO_2$) qui ont des effets significatifs sur la santé et l'environnement. En tenant compte de cette situation, il est essentiel de développer des procédés innovants pour la production d'énergies renouvelables. Parmi ces procédés, la méthanation biologique apparait comme technologie prometteuse à la fois pour la production du méthane ($CH_4$) et le réemploi du $CO_2$.

**Le bio-méthane est-il vraiment la source d'énergie de transition dont le monde a besoin ?**
**La productivité en méthane répond-elle aux besoins nationaux et mondiaux?**

## Solution

Le bio-méthane est perçu comme très prometteur dans le monde des énergies renouvelables. Il possède des propriétés identiques à celles du gaz naturel et peut donc le remplacer, tout en ayant moins d'impact sur l'environnement. S'il peut être produit par épuration du biogaz de méthanisation à partir de déchets organiques, la méthanation qui permet de produire du méthane à partir de $CO_2$ et de $H_2$ est une alternative intéressante, mais son rendement est actuellement faible.

L'objectif général du projet est d'améliorer un procédé continu de méthanation biologique ex-situ pour produire du méthane en optimisant des paramètres d'influence tel que le transfert de matière liée en particulier la faible solubilité dans l'eau du $H_2$ gazeux.

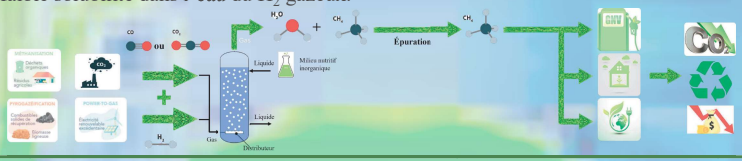


## Maquette froide

**Colonne à bulles**
- PVC transparent
- $\varnothing_i$ = 54 cm
- Réservoir de compensation de réfraction

**2 caméras rapides**
- Modèle : Chronos 1.4
- Résolution max : 1280 x 1024 à 1069 fps

**Pompe péristaltique**
- Modèle : SHENCHEN LabS3
- Débit max : 790 ml/min
- Liquide : eau distillée

**Diffuseur de bulles**
- Acier inox fritté
- Céramique frittée

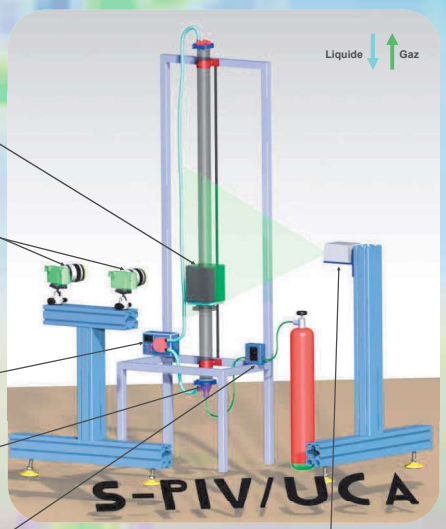


**Régulateur de débit massique**
- Modèle : (MFC) D-6311
- Gamme de débit : 0-250 $ml_n$/min
- Gaz : air

Laser « **MGL-N-532nm-4W** »

## Méthode

Réactions : $\begin{cases} CO_{2\,(g)} + 4H_{2\,(g)} \rightleftarrows CH_{4\,(g)} + 2H_2O_{(g)} & \Delta_r H = -165\ \mathrm{KJ}/mol_{298K} \\ CO_{(g)} + 3H_{2\,(g)} \rightleftarrows CH_{4\,(g)} + H_2O_{(g)} & \Delta_r H = -206\ \mathrm{KJ}/mol_{298K} \end{cases}$

**Étude expérimentale**

❖ Hydrodynamique locale en fonction de :
- Conditions opératoires (débits de gaz et de milieu)
- Mode de fonctionnement du réacteur
- Paramètres géométriques (distributeur de gaz, présence d'inserts)

❖ Temps de mélange : $t_m$

❖ Taux de gaz : $\tau_g$

❖ Transfert de matière gaz-liquide : solubilité de $H_2$

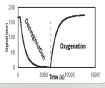


**Modélisation & simulation numérique (CFD)**
- Modélisation de l'hydrodynamique
- Modélisation du transfert de masse

CHAM PHOENICS

Proposition d'améliorations pour l'intensification du procédé dans la maquette chaude

## Résultats

- Liquide : eau distillée
- Gaz : air
- Débit $_{gaz}$ : 150 ml/min
- Débit $_{liquide}$ : 0 ml/min

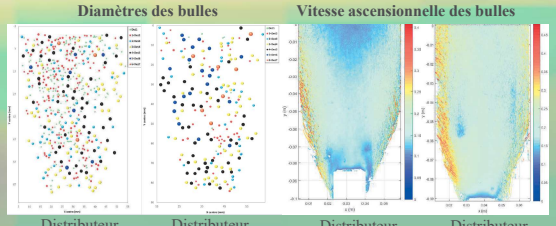


## Conclusion & futur travail

➢ Le distributeur céramique génère plus de bulles que le métallique
➢ Le distributeur céramique crée des bulles plus petites que le métallique, ce qui explique les vitesses ascensionnelles plus élevées dans le cas du frittée métallique
➢ L'étape suivante est la mesure du taux de gaz avec les différents distributeurs pour pouvoir calculer le coefficient de transfert de matière gaz-liquide

**Remerciements :** Ce travail est financé par le Programme **Pack Ambition Recherche** de la région Auvergne Rhône Alpes (**projet ProMethEx**)

# Biological oxygen production and air revitalisation for habitats on the Moon


**Jana Fahrion**

*SCK-CEN in Mol, Belgium in collaboration with UCA in Clermont-Ferrand, France*
*Promoter: Prof. Dr. Claude-Gilles Dussap (UCA)*
*Mentor: Dr. Natalie Leys (SCK CEN)*

Ecole doctorale Sciences Pour l'Ingénieur


## Introduction

In this PhD project, we are investigating biotechnology for space, capable of functioning under cosmic radiation. This project is part of the ArtEMISS project (Arthrospira sp. gene Expression and mathematical Modelling on cultures grown in the International Space Station) and the MELiSSA program (Micro-Ecological Life Support System Alternative) from the European Space Agency (ESA). MELiSSA aims to recycle the wastes of space travellers (e.g. faeces, urine and $CO_2$) to produce new edible biomass, potable water and oxygen ($O_2$) for space craft crews. The ArtEMISS project is focussing on biological air revitalisation and food production via a photobioreactor containing an edible photosynthetic cyanobacterium called *Limnospira indica* PCC8005. It is our aim to transplant this photosynthetic microbial bioprocess to space, where exposed to cosmic radiation and reduced gravity, via a pilot flight experiment on board ISS called ArtEMISS-C. A detailed review of the use of photobioreactors in space can be found in Fahrion et al. 2021.

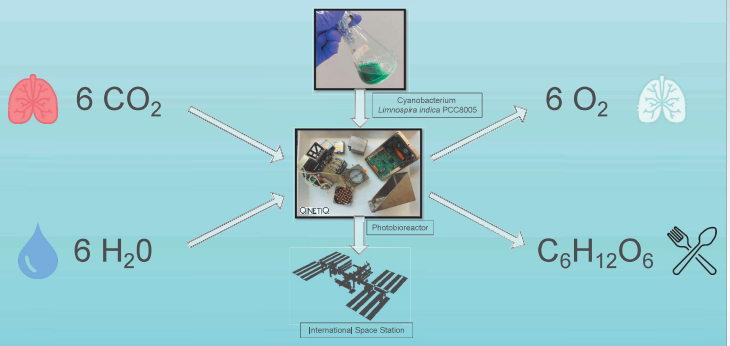


## Methods

For the tests on different growth conditions, cyanobacterium *L. indica* strain PCC8005 subculture P3 was grown in Zarrouk's medium as modified by Cogne et al. (2003). Depending on the experiment, different temperatures (23–34°C) and several light intensities (36–140 µE $m^{-2}$ $s^{-1}$) were used. The cultures were constantly illuminated with full PAR emitting light sources (LEDs and halogen lamps) in all experiments. All experiments were conducted in Erlenmeyer flasks (batch cultures). The growth was followed via $OD_{770nm}$ and dry weight measurements. A detailed description of the methods and results of the influence of light and temperature can be found in Fahrion et al. 2023.

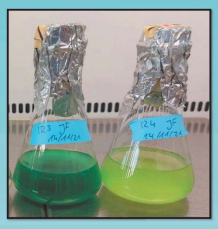

For our irradiation experiments, the cyanobacterium *L. indica* strain PCC8005 subculture P3 was grown in Zarrouk's medium in 250 mL Erlenmeyer flasks (150 mL culture volume). Two experiments were performed, one with 4 batches (2 weeks each, 5% inoculation), one with 8 batches (1 week each, 25% inoculation). The cultures were constantly illuminated with full PAR emitting light sources (LEDs) at 45 µmol photons $m^{-2}$ $s^{-1}$ and at 25°C. In both experiments irradiation was applied using a $Co^{60}$ source (75 µGy $h^{-1}$). This dose rate mimics a transit to Mars inside of a space vehicle (Hassler et al. 2014) The growth was followed via $OD_{770nm}$, pH and dry weight measurements.

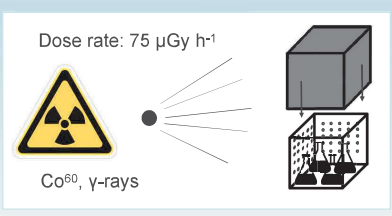


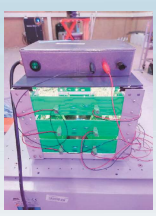

Set-up of the irradiation experiment, a cover was used to shield the cultures from additional light in the room

## Results

Influence of different light intensities and temperatures on the biomass production and maximum phycocyanin content of *L. indica:* The lower light intensities reached higher maximum biomass yields, and the temperature had the biggest impact on the biomass production at I = 140 µE $m^{-2}$ $s^{-1}$ (1,6 ± 0,1 g/L [34°C] vs. 0,8 ± 0,1 g/L [25°C]). The content of the antenna pigment phycocyanin was highest in the cultures grown at low light (36-75 µE $m^{-2}$ $s^{-1}$) and high temperature (30-34°C)

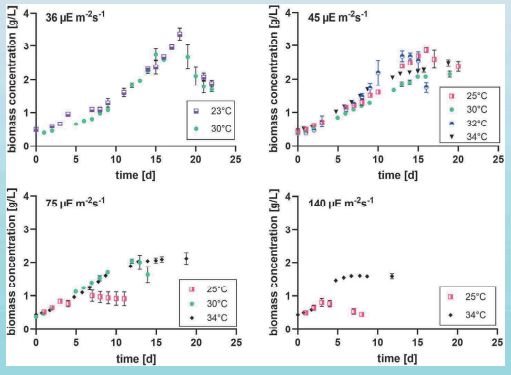


| Max. phycocyanin [g g DW$^{-1}$] | 36 µE $m^{-2}$ $s^{-1}$ | 45 µE $m^{-2}$ $s^{-1}$ | 75 µE $m^{-2}$ $s^{-1}$ | 140 µE $m^{-2}$ $s^{-1}$ |
|---|---|---|---|---|
| 23°C | 0.030 ± 0.003$^{ad}$ | - | - | - |
| 25°C | - | 0.077 ± 0.004$^{c}$ | 0.025 ± 0.004$^{d}$ | 0.018 ± 0.004$^{d}$ |
| 30°C | 0.122 ± 0.014$^{b}$ | - | - | - |
| 32°C | | 0.123 ± 0.013$^{b}$ | - | |
| 34°C | - | 0.130 ± 0.009$^{b}$ | 0.129 ± 0.008$^{b}$ | 0.051 ± 0.017$^{a}$ |

Influence of long-term low-dose irradiation on the dry weight: The irradiated cultures were growing faster in batch 2 of exp. 1. In exp. 2, this transient hormesis effect is less pronounced, only after 4 weeks the irradiated cultures showed a significantly higher dry weight.

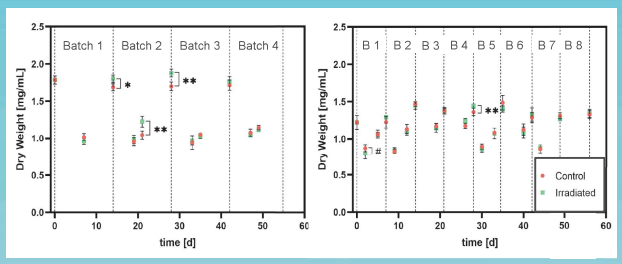


## Conclusions

A low light intensity (36 - 80 µE $m^{-2}$ $s^{-1}$ ) in combination with warm temperature (34°C) can be used to obtain a well controllable culture with a high pigment content and a high biomass production in a batch culture.

*Limnospira indica* PCC8005 P3 shows a transient hormesis effect under chronic low-dose gamma irradiation in batch cultures. These results give a first indication that the cultures will likely not be impacted negatively by a flight to Mars.

### Published results in international journals


1) Fahrion, J., Mastroleo, F., Dussap, C. G., & Leys, N. (2021). Use of photobioreactors in regenerative life support systems for human space exploration. *Frontiers in microbiology*, *12*, 699525.
2) Fahrion, J., Dussap, C. G., & Leys, N. (2023). Assessment of batch culture conditions for cyanobacterial propagation for a bioreactor in space. *Frontiers in Astronomy and Space Sciences*, *10*, 1178332.


### Acknowledgements


This study was sponsored via the ESA ARTEMISS prodex contract and is part of the MELiSSA program of ESA, in the context of a PhD program of SCKCEN

# Deep learning Analysis of multiprobe sensors network to assess risk scenarios at volcanic hydrothermal systems

Michail Giannoulis[a], Andrew Harris[b], Vincent Barra[a]
[a]Université Clermont-Auvergne, CNRS, Mines de Saint-Étienne, Clermont-Auvergne-INP, LIMOS, 63000 Clermont-Ferrand, France.
[b]Université Clermont-Auvergne, CNRS, LMV, 63000 Clermont-Ferrand, France

Ecole doctorale Sciences Pour l'Ingénieur

## Introduction

Volcanoes are nature's ticking time bombs, periodic examination for abnormalities is crucial. The subject of this work is *Vulcano.* A composite volcano located at Aeolian islands, on which numerous meteorological and surface (1D) sensors are installed to record its behavior on every five minutes.

## Research Objective

This thesis focus on the development of DITAN; a framework to detect and interpret temporal-based anomalies as critical regions on a multi-sensor time series. It is built upon the assumption that normality is identical to regularity, where irregular records are considered temporally less predictable than regular ones.

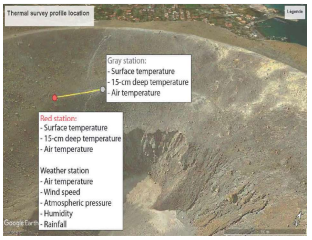


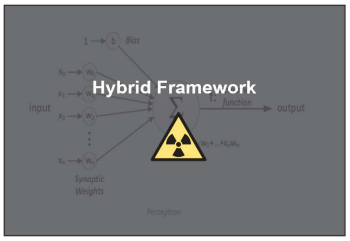


Critical Regions

| Deep Learning (DL) | Expert System (ES) |
|---|---|
| **Detect abnormal values** | **Interpret into physical (sensor) events** |

## Deep Learning (DL)

We propose an encoder-decoder architecture with both implicit and explicit attention, trained in an unsupervised manner using bayes optimizer. It learns to predict normality formulating regular and irregular patterns. The irregular ones are the critical (full/sub space) regions in which anomalies allocated.

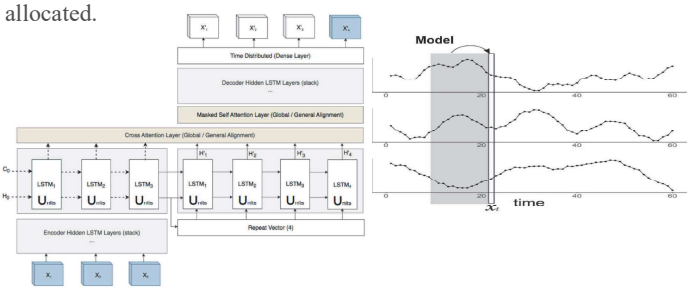


*From sensor values to the formation of critical regions*

## Expert System (ES)

We propose an expert system that enables experts to CRUD temporal if-then rules and apply reasoning in an online environment. An event-driven inference engine do all the complex procedure of mapping rules to the critical regions.

**Algorithm 1** Inference Engine

**Require:** $KB, CR$ ▷ Knowledge Base (KB), Critical Regions (CR)
**Ensure:** $ED$ ▷ Events Base (EB)
$\epsilon \leftarrow 0$ ▷ number of events allowed in rule's precondition
$RM \leftarrow []$ ▷ maintain the total valid rules
**while** $True$ **do**
  $rules \leftarrow FetchRules(KB, \epsilon)$ ▷ Fetch rules ordered by the number of events
  **if** $len(rules) == 0$ **then** ▷ Halt if there are no more rules
    *break*
  **end if**
  **for** $R \in rules$ **do**
    $durations \leftarrow RuleExcerets((CR, EB, R)$
    **If** $durations \neq []$ **then** ▷ find all duration in which the rule is validated
      $EB.update([R : durations])$ ▷ Keep only the executed rules
    **end if**
  **end for**
  $\epsilon \leftarrow \epsilon + 1$ ▷ increase number of events for the next iteration
**end while**

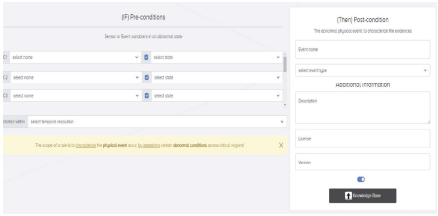


*From critical regions and rules to physical events*

## Preliminary Results

| | P | R |
|---|---|---|
| MERLIN [33] | 0.9846 | 0.4913 |
| LSTM-NDT [16] | 0.9207 | 0.9718 |
| DAGMM [53] | 0.9475 | 0.9900 |
| OmniAnomaly [39] | 0.8561 | 1.0000 |
| MSCRED [48] | 0.9272 | 1.0000 |
| MAD-GAN [22] | 0.9396 | 1.0000 |
| USAD [2] | 0.8953 | 0.9989 |
| MTAD-GAT [54] | 0.9018 | 1.0000 |
| CAE-M [55] | 0.8442 | 0.9997 |
| GDN [10] | 0.8832 | 0.9892 |
| TranAD [52] | 0.9569 | 1.0000 |
| DITAN (our) | 0.9910 | 0.7785 |

Precision and Recall of DITAN model w.r.t. state of the art

The reasoner identified two physical events, *rainstorm* and *low-pressure system,* both happened in March 24 at different duration. These two events occur since, (Expert) rule preconditions successfully satisfied upon the (Model) critical regions. Note that the truth of the result is also validated by the experts.

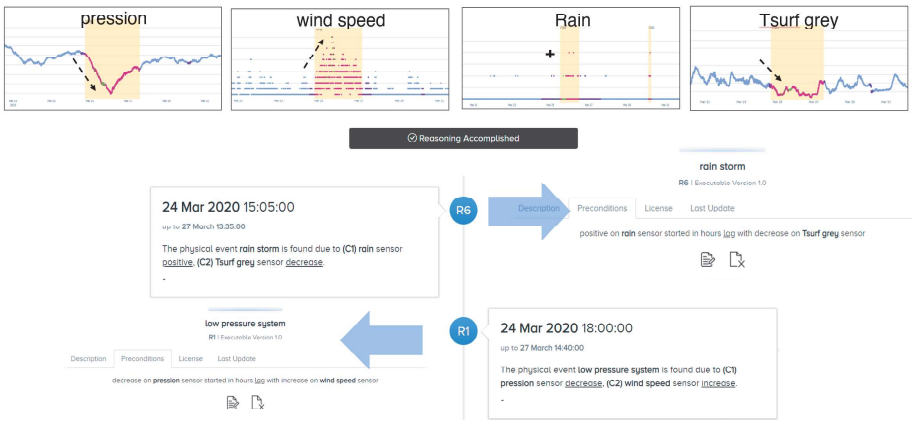


## Future work

- Add a new module to predict abnormality, trained in a supervised way using our DITAN model
- Support 2D input formats (e.g., image data)

## References

K. Hundman et al. Detecting spacecraft anomalies using lstms and nonparametric dynamic thresholding. In Y. Guo and F. Farooq, editors, Proc. of the 24th Int. Conf. on KDD, 387–395. ACM, 2018.

M.Giannoulis, A. Harris, V. Barra, A Domain-Agnostic Framework of Temporal-based Anomaly Detection and Interpretation for Multivariate Sequential Data, pattern recognition (accepted)

This project is supported by ANR (ANR-19-CE04-0014-01 DIRE)

# Faisabilité de la rénovation des bâtiments français dans un contexte perturbé


**Marceau GOUROVITCH[1,2]**

Directeur de thèse : Jean-Philippe COSTES[2] | Co-encadrant : Bertrand LARATTE[3]

*1 : C-TEK Ingénierie, St Thibault des Vignes, France*
*2 : UCA/ENSACF/Ressources, Clermont-Ferrand, France*
*3 : Arts et Métiers, Université de Bordeaux, CNRS, Bordeaux INP, INRAE, I2M Bordeaux, Talence, France*

Ecole doctorale Sciences Pour l'Ingénieur


## Introduction

- 3 perturbations majeures en cours : changement climatique, diminution de l'approvisionnement énergétique et nexus consommation-production-approvisionnement en ressources.
- Ces trois perturbations vont s'accélérer.
- Le « Plan rénovation énergétique des bâtiments » prévoit de rénover **500 000 logements** par an.
- Actuellement, le chiffre oscille entre **10 000 et 70 000 logements** par an.
- Il faut des matériaux permettant d'être résilient face aux trois perturbations tout en tâchant de répondre au plan de rénovation.

## Objectifs

1. Caractériser la production française de matériaux biosourcés.
2. Étudier la compatibilité entre le plan de rénovation et la production de matériaux.
3. Étendre l'étude à la compatibilité entre la rénovation de tous les bâtiments et la production de matériaux.
4. En fonction des résultats proposer une feuille de route pour la rénovation des bâtiments.

## Méthodologie

**Faisabilité du plan de rénovation des logements**

Étape 1 : Choix des matériaux
Ⓟ Choix basé sur les hypothèses introductives des perturbations.

Étape 2 : Définition des matériaux choisis
Ⓟ Connaitre plus précisément les matériaux afin de catégoriser leur utilisation (un isolant est différent d'un matériau de structure)

Étape 3 : Caractérisation de la quantité produite actuelle et future de ces matériaux en France

Étape 4 : Convertir ces quantités produites en nombre de logements rénovés (ou mètres carrés rénovés)
Ⓟ Connaitre la possibilité réelle de rénovation basée sur le stock

Étape 5 : Discussion sur les résultats

**Faisabilité d'un plan de rénovation des bâtiments français (logements, tertiaire, ERP, etc.)**

Étape 1 : Quantification des bâtiments à rénover
Ⓟ Distinguer les bâtiments tertiaires de type bureau des bâtiments tertiaires type ERP (bâtiments publics, enseignement, etc.)

Étape 2 : Quantification des besoins en matériaux
Ⓟ En fonction des bâtiments, le besoin en matériaux n'est pas le même.

Étape 3 : Discussion sur les résultats

## Difficultés

- Quantifier la production des matériaux
- Quantifier le nombre de rénovations à effectuer en fonction des types de bâtiment
- Quantifier la quantité de matériaux nécessaire pour la rénovation en fonction du type de bâtiment

## Premiers résultats

Matériaux résilients aux perturbations et faisant donc l'objet de l'étude :

Paille — Chanvre — Bois — Ouate de cellulose

Résultats pour la paille :

| | Seegers et al. | ONRB | Mourjane et Fosse |
|---|---|---|---|
| Production (Mt) | 3,9 | 2,23 | 2,99 |
| MI rénovables | 433 333 | 247 778 | 332 222 |
| soit du parc MI | 2,2% | 1,2% | 1,6% |

Nota : il y a 20 137 000 maisons individuelles en France
MI : maison individuelle

## Suite de l'étude

Développer la méthodologie pour :

- Avoir les résultats de production pour chaque matériau ;
- Connaitre la possibilité matérielle de rénovation du parc de bâtiments français ;
- Discuter et critiquer les résultats ;
- Faire des propositions en conséquence.

Discussion : 2 cas possibles
1 : quantité de matériaux insuffisante
  ☾ Propositions pour combler ce manque
2 : quantité de matériaux suffisante
  ☾ Proposition et ouverture vers d'autres facteurs bloquants (main d'œuvre, politique, etc.)

## Bibliographie


MTES et MCT, « Plan rénovation énergétique des bâtiments » (La Défense: MTES-MCT, octobre 2017).
SEEGERS J et al., « Autonomie en paille et poids économique des achats de litières dans les élevages en France : analyse rétrospective des données INOSYS Réseaux d'élevage 2001-2020 », no 26 (2022): 529-33.
ONRB, « Disponibilité en pailles de céréales 2021 », décembre 2022
Ilyas Mourjane et Julien Fosse, « La biomasse agricole : quelles ressources pour quel potentiel énergétique ? » (Paris: France Stratégie, juillet 2021), www.strategie.gouv.fr

# Automatic detection of anomalies in the circadian rhythm of dairy cows

Valentin GUIEN

Supervised by: Koko J., Antoine V., Veissier I., Lardy R.

## Background

**Precision Livestock Farming** is based on various **numerical techniques** applied to data that is usually collected routinely thanks to sensors. It provides the farmer with information to **anticipate** situations requiring action on animals, buildings, etc.

Figure 1: A cow with a CowView sensor on its collar detecting its activity

## Circadian cycle

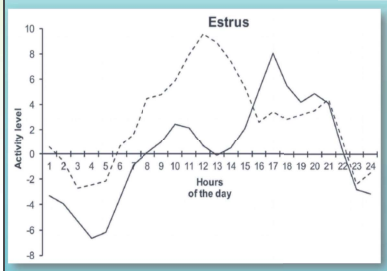


Figure 2: Circadian cycle of activity of a cow in 'normal days' (solid line) vs. in estrus (dotted line) [1]

The **circadian cycle** of animals expresses a specific rhythm of activity (eating, moving, resting, etc.). A change in the rhythm of activity is an indicator of a **change** in the animal's internal state due to **disease, stress** or a particular **physiological** condition [1].

The aim is to **detect** changes in these circadian cycles that may be precursors to a change in the cow's **internal state**.

## Challenges

Specific data-related difficulties:

- **Inter-individual** variability: two cows will behave differently.
- **Intra-individual** variability: the activity of a given cow varies from day to day.
- Many possible **perturbations**, with a variety of **consequences**, of which we don't have full knowledge.

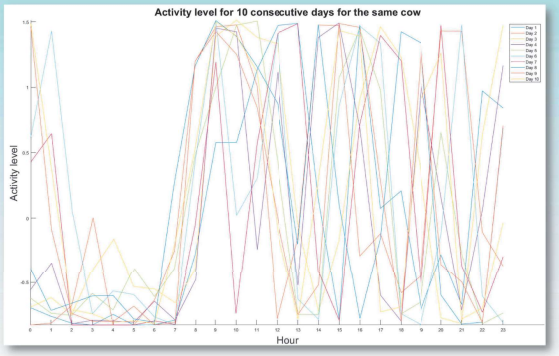


Figure 3: 10 consecutive circadian cycles of activity of a cow

## Simulation

The current dataset is :

- **Limited**: Not much data due to intra-individual variability.
- **Uncertain**: We are not sure about the labelling of cow internal state because of this variability.

Solution : Create a model to **simulate** a cow behavior, based on a **Markov** model.

Figure 4 : A cow resting in a cubicle, Marcenat

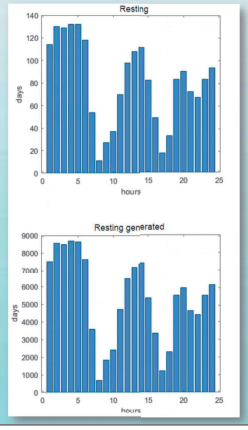


Figure 5: Distribution of resting, real data vs. generated data

Other **criteria** must be found to **validate** the simulations (tests, boxplot,...).

## Wavelet transform

Previous work [2] was based on the Fourier transform (**FBAT method**) to detect anomalies in time series. **Wavelet transforms** are better suited to **non-stationary** series.

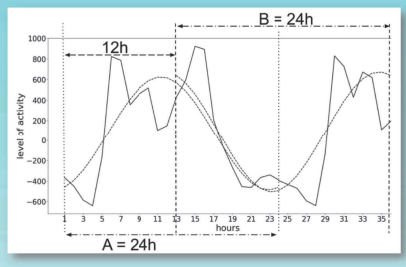


Figure 6: Comparison of two sub-series with FBAT method [2]

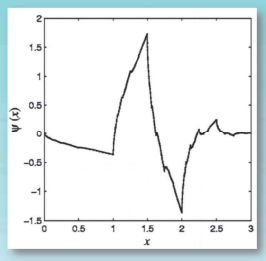


Figure 7 : Daubechies Wavelet [3]

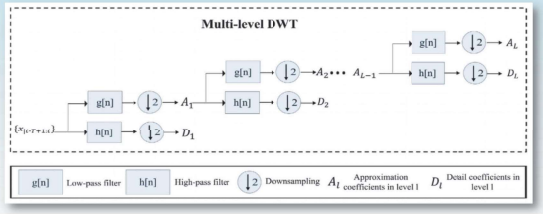


Figure 8 : Multi-level Discrete Wavelet Transform Processes [4]

## References

1. Veissier, I., Mialon, M.-M. and Helle Sloth, K., 2017 "Short communication: Early modification of the circadian organization of cow activity in relation to disease or estrus". Journal of Dairy Science 100, n° 5.
2. Wagner, N., Mialon, M.-M, Helle Sloth, K., Lardy, R., Ledoux, D., Silberberg, M., De Boyer Des Roches, A. and Veissier, I., 2021 "Detection of Changes in the Circadian Rhythm of Cattle in Relation to Disease, Stress, and Reproductive Events", Methods 186:14-21
3. Cole, M., Keogh, P.s., Burrows, C.R. and Sahinkaya, M. N., 2006 "Adaptive Control of Rotor Vibration Using Compact Wavelets". Journal of Vibration and Acoustics 128, n° 5: 653-65.
4. Yao, Y., Ma, J., et Ye, Y., 2023"Regularizing autoencoders with wavelet transform for sequence anomaly detection". Pattern Recognition 134

# Prise en compte des incertitudes dans la rénovation vers des bâtiments à énergie nette nulle

Mahdi IBRAHIM[a,b], Farouk FARDOUN[b], Fatima HARKOUSS[c], Pascal BIWOLE[a,d], Salah OULDBOUKHITINE[a]

a Université Clermont Auvergne, CNRS, SIGMA Clermont, Institut Pascal, F-63000 Clermont–Ferrand, France
b Université Libanaise, Centre de Modélisation, Ecole Doctorale des Sciences et Technologie, Hadat, Lebanon
c Al Maaref University, Faculty of Engineering, Beirut, Lebanon
d MINES Paris Tech, PSL Research University, PERSEE - Center for Processes, Renewable Energies and Energy Systems, CS 10207, 06 904 Sophia Antipolis, France

## 1-Introduction

- Consommation d'énergie élevée:
  - Le secteur du bâtiment représente 44 % de l'énergie totale consommée en France
  - Solution: Bâtiment a Energie Nette Nulle

Rénovation Energétique du Bâtiment

- Problématique et contexte:

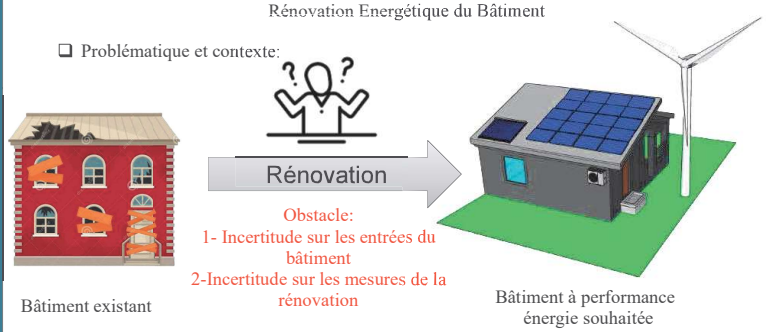


- Différents paramètres d'entrée des mesures de rénovation peuvent entraîner une incertitude quant aux performances énergétiques après leur mise en place

## 2-Méthodologie

Calibration des simulations

Calibration de la simulation énergétique d'un bâtiment avec les données mesurées afin de résoudre les incertitudes liées aux entrées du bâtiment

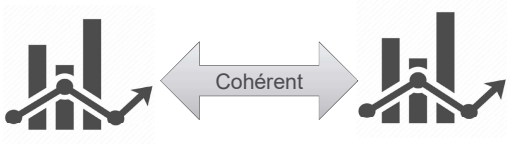


analyse de la sensibilité

Sélectionner les mesures de rénovation les plus influentes sur la consommation d'énergie par méthode du SOBOL


Analyse de l'incertitude

Quantifier l'influence des paramètres incertains sur la performance énergétique du bâtiment par Monte Carlo Simulation

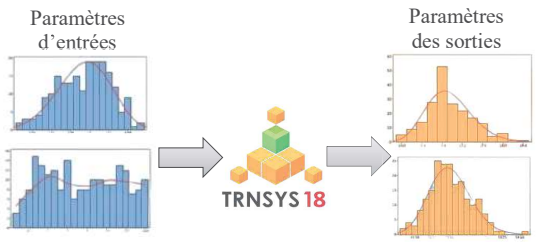


## 3-Cas d'étude

Bâtiment existant étude

Station météorologique

Les humidités, températures extérieures et intérieures ont été enregistrées chaque heure.

## 4-Premiers Résultats

Les humidités intérieures ont été calibrées pour 9 mois

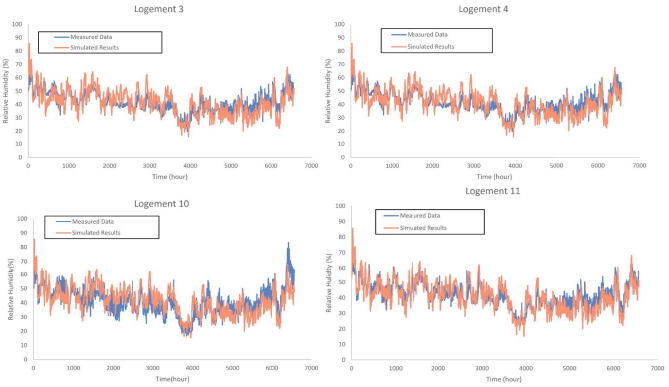


## 5-Conclusion

- Les résultats simulés calibrés et les données expérimentales sont cohérents selon la norme ASHRAE 14.
- Des efforts seront déployés afin de calibrer le modèle de manière à obtenir une compatibilité avec la température et la consommation de chauffage fournies par les capteurs.
- Après avoir finalisé cette étape, une analyse de sensibilité et des incertitudes seront déployées.
- Optimisation des mesures de rénovation doit être établie afin de réaliser un bâtiment à énergie nette nulle.
- Utilisation d'un machine Learning model afin de minimiser le temps de calcul dans l'optimisation.
- La méthodologie sera appliquée à plusieurs climats.

## 6-Bibliographie

1. « L'énergie en France », Agir pour la transition écologique | ADEM
2. K. Binder et D. W. Heermann, Monte Carlo simulation in statistical physics: an introduction, 5th ed. Heidelberg ; New York: Springer, 2010.
3. R. Heijungs et M. A. J. Huijbregts, « A Review of Approaches to Treat Uncertainty in LCA ».

## 7-Remerciements

Ce travail de recherche est soutenu par le financement du Département de l'Allier.


Contact: mahdi.ibrahim@doctorant.uca.fr

# *CYSTOSTEIRA BACCATA A* BROWN SEAWEED FROM MOROCCO'S ATLANTIC COAST: METABOLITES AND BIOREFINERY SCENARIO

Ibtissam SABIR [1,2,3*], Halima RCHID [2], Alina-Violeta URSU[1], Philippe MICHAUD[1], Lucia BRAGA NAN[1], Pierre FONTANILLE[1], Guillaume PIERRE[1], Cedric DELATTRE[1], Christine GARDARIN[1], Rachid NMILA [2], Reddad EL MOZNINE [3] Christophe VIAL[1]

[1]Clermont Auvergne University, Pascal Institution, CNRS, Clermont-Ferrand, France.
[2]Biotechnology And Valorization Of Vegetal Resources, Faculty Of Sciences, Chouaib Doukkali University, El Jadida, Morocco
[3]Laboratory Physics of Condensed Matter, Faculty Of Sciences, Chouaib Doukkali University, El Jadida, Morocco

* Corresponding author: ibtissam.sabir@doctorant.uca.fr

## Introduction

• The Moroccan coast presents an undeniable richness in terms of diversity and quantity of macroalgae, in El Jadida coast: 86 algal species were identified only on 110km) [1].
•Due to their large variety of metabolites, *Cystoseira* genus is an important brown seaweed that could provide sustainable alternative sources of food, feed, chemicals, energy and materials.

**Goal of the study: Biorefinery of *Cystoseira* seaweed**

**Polysaccharides**

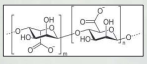

Alginate

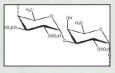

Fucoïdan

**Phenolic compounds**

**Lipids**

*C. baccata*

**Energy Carriers**

○ **Bio-$H_2$**

○ **Bio-$CH_4$**

## Methods

•**Seaweed pre-Treatement:** algae biomass harvested from the coast of Sidi Bouzid, El Jadida (33 ° 09'-33 °16"N, 8 ° 30'-8 ° 45'W) was washed, dried at 45 °C ± 2°C, ground into powder and sieved.

• **Extraction and Purification of Polysaccharides (Alginates and Fucoidans)**

**Dried algal biomass**

Acetone | Methanol

**Depigmentation / Deffating**

HCl | Treatment

**Residue** | **Supernatant**

$Na_2CO_3$ | Treatment

**Supernatant**

Acidification | with HCl

**Alginic acid**

Neutralization | with NaOH

**Sodium alginate**

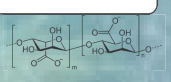

**Fucoidan**

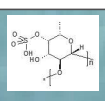

## Methods

- **Lipids Extraction:** performed by Soxhlet extractor, using hexaneas solvent
- **Phenolic Compounds extraction:** performed by methanol/water under stirring.
- **Biochemical Methane Potential:** *Cystoseira sp.* substrate is mixed with an inoculum (anaerobic bacteria culture retrieved from an active digester)

## Results

- **Polysaccharides extraction yield** depend on biomass particle size (*see Table*). The yield of alginates is close to those described in literature for other species of *Cystoseira sp.*, such as *C. compressa* (21.65%) [2], and *C. barbata* (9.9%) [3]. The same trend was observed for fucoidans[4].

- **BMP** results applied for *Cystoseira baccata* show that the CH4 production strongly depends on the species (Tab. 1).

***Extraction yield of Alginate and Fucoidans obtained from C.baccata***

| Sample size (average diameter, µm) | Alginate yield (%) | Fucoidan yield (%) | BMP ($Nm^3CH4/T$ organic matter) |
|---|---|---|---|
| Tiller: 1000 | 18.6 | 2.6 | n.d. |
| Powder: 900 | 24.6 | 2.0 | n.d. |
| Powder: 570 | 24.1 | 1.8 | n.d. |
| Powder: ~300 | 19.5 | 1.9 | n.d. |
| Fine powder (<125) | 10.5 | 3.2 | **1065.0** |

- **Lipids extraction yield** of *C. baccata* is close to 2% (wt./wt dry weight).
- Higher yield is detected for **phenolic compounds**: 17.8% (wt./wt., dry weight basis) compered to other brown algae [5].

## Conclusions

•This study shows that *C. baccata* from the Maroccan Atlantic coast (Sidi Bouzid coast) contains important amounts of high added-value biomolecules, such as alginates, fucoidans, lipids and phenolic compounds.
•the biomass feedstocks, whole or extracted wastes (in progress) present good potential for the supply of energy carriers, such as bioH2 and bioCH4 by dark fermentation and anaerobic digestion, respectively.

## Bibliography

[1]. Chibi F. et al., Screening of the antioxidant activity of crude extracts in 86 algae species from El Jadida coast (Morocco), *Int. J. Pharm. Pharm. Sci.*, 22, (2019), 54-61.
[2]. Hentati F. et al., Structural characterization and antioxidant activity of water-soluble polysaccharides from the Tunisian brown seaweed *Cystoseira compressa*, *Carbohydr. Polym.*, 198, (2018), 589-600.
[3]. Sellimi S. et al., Structural, physicochemical and antioxidant properties of sodium alginate isolated from a Tunisian brown seaweed, *Int. J. Biol. Macromol.*, 72, (2015), 1358-1367.
[4]. Sellimi S. et al, Fucans from a Tunisian brown seaweed *Cystoseira barbata*: Structural characteristics and antioxidant activity, *Int. J. Biol. Macromol.*, 66, (2014), 281-288.
[5]. Connan S. et al., Interspecific and temporal variation in phlorotannin levels in an assemblage of brown algae, *Bot. Mar., 47, 5,* (2004), 410-416.

## Acknowledgement:

this work was financially supported by Campus France through Hubert Curien Partnership.

# Multimodal Tumour Registrations and Augmentations

Ecole doctorale Sciences Pour l'Ingénieur

M. Mahdi KALANTARI,
Erol OZGUR, Mohammad ALKHATIB, Youcef MEZOUAR, Adrien BARTOLI

*Mohammad_Mahdi.KALANTARI@doctorant.uca.fr*

IMMORTALLS

## Introduction

Liver cancer is one of the leading causes of cancer deaths worldwide. An estimated 900,000 people around the world were diagnosed with the disease in 2020.

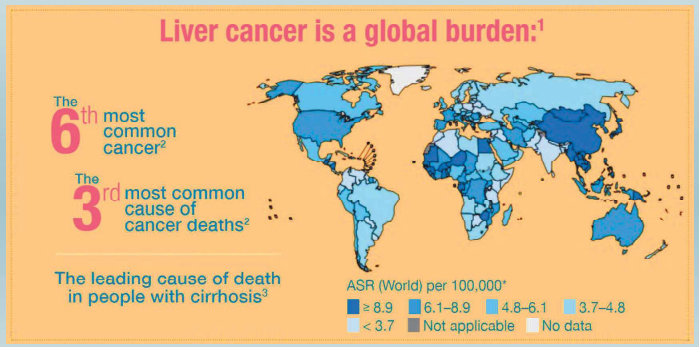


Adopted from [1]

Laparoscopic liver resection (LLR) is the main treatment, but challenging:
(i) intraoperative bleeding,
(ii) unable to palpate,
(iii) long learning curve of laparoscopic ultrasound (LUS)

Augmented reality can mitigate these problems by visualizing veins and tumors and fusing ultrasound data directly into the surgical image.

## Project Goals

The main goal of the project is to provide a *practical* approach to the problem. By satisfying the below targets, the solution would be *practical* and close to ideal:

1. **Realtime**: Augmentation must be performed fast enough that surgeons do not sense any lag between the movements in the surgical image and the augmented objects.
2. **Automatic**: No manual initialization must be required to start the algorithm.
3. **Utilizing no additional sensors**: The operating room must be left intact because adding sensors limits the applicability of the system.
4. **Utilizing no additional markers**: Same as sensors, adding markers to the devices or the body of the patient requires extensive considerations that reduce the ability of the system to be practical

When all these goals are met, the result of the project can be used in a normal operating room with leaving the devices as it is.

## State of the Art

To the best of our knowledge, there is no work in the literature that satisfies all the aforementioned goals of the project and at least, they violate one of them. To be more precise, [2,3] are not real-time and [4,5] are not automatic. Most of the works in the field use markers and trackers to perform the registration that [6,7] are the recent examples.

## Methodology

With Computerized Tomography (CT) or Magnetic Resonance Imaging (MRI) of the patient before the surgery, there is a preoperative model of the liver and the tumour(s) available. But direct augmentation from the preoperative model to the surgical is tested before [8] and it is computationally complicated that cannot be real-time and automatic.
To overcome this problem, LUS can be incorporated as a proxy that minimizes the registration volume and it can be registered to the surgical image rigidly because it is recording data synchronized with the surgical image.

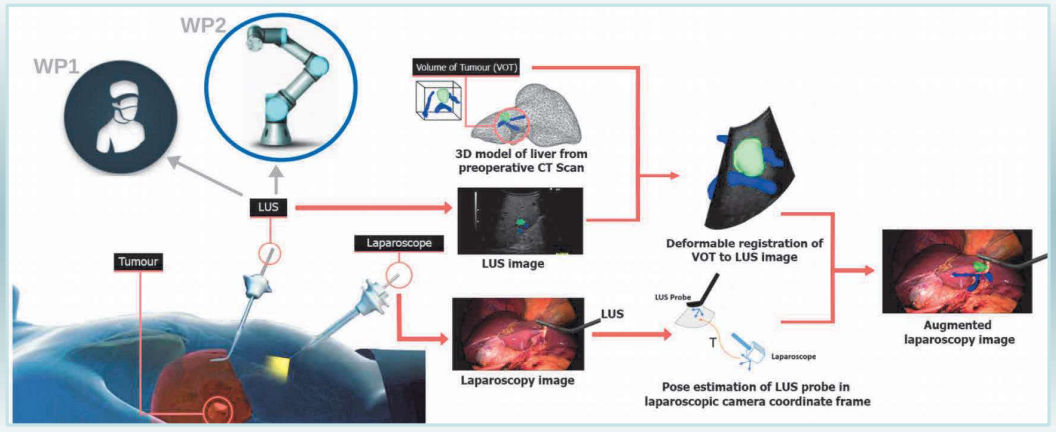


## Expected Contributions

The principal purpose of the project is to abate the mortality rate of liver cancer. In this way, multiple scientific contributions can be made in different fields:

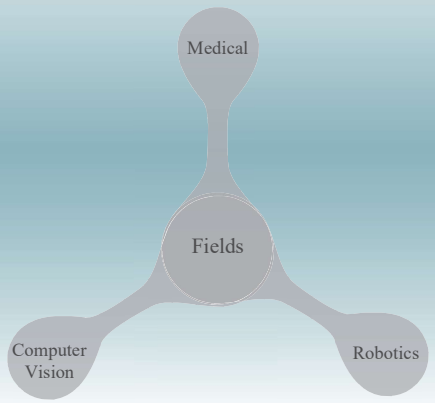


## Bibliography

[1] https://easlcampus.eu/infographics/liver-cancer-explained

[2] N. Montaña-Brown *et al.* "Vessel segmentation for automatic registration of untracked laparoscopic ultrasound to CT of the liver". *Int J CARS* 16, 1151–1160, 2021.

[3] J. Ramalhinho *et al.* "Deep hashing for global registration of untracked 2D laparoscopic ultrasound to CT". *Int J CARS* 17, 1461–1468 2022.

[4] J. Ramalhinho *et al.* "Registration of Untracked 2D Laparoscopic Ultrasound to CT Images of the Liver Using Multi-Labelled Content-Based Image Retrieval," in *IEEE Transactions on Medical Imaging*, vol. 40, no. 3, pp. 1042-1054, March 2021

[5] B.R. Thomson *et al.* "MR-to-US Registration Using Multiclass Segmentation of Hepatic Vasculature with a Reduced 3D U-Net". In: Medical Image Computing and Computer Assisted Intervention – MICCAI 2020.

[6] E. Pelanis, *et al.*, "Evaluation of a novel navigation platform for laparoscopic liver surgery with organ deformation compensation using injected fiducials," Medical Image Analysis, Vol 69, 101946, ISSN 1361-8415, 2021

[7] X. Liu *et al.* "Hybrid electromagnetic-ArUco tracking of laparoscopic ultrasound transducer in laparoscopic video", *Journal of medical imaging (Bellingham, Wash.)*, *8*(1), 015001, 2021

[8] Y. Espinel, E. Özgür, L. Calvet, B. Le Roy, E. Buc, A. Bartoli, "Combining Visual Cues with Interactions for 3D-2D Registration in Liver Laparoscopy." *Annals of biomedical engineering*, *48*(6), 1712–1727, 2020

# Learning Multivariate Time Series

*Applications to tire manufacturing and wear prediction*

*(In collaboration with Michelin)*


**Thabang Lebese**[1]

**Supervised by: C. Mattrand**[2]**; D. Clair**[3]**; JM. Bourinet**[4]**; F. Deheeger**[5]

[1,4]LIMOS; [2,3,4]SIGMA Clermont; [2,3]Institut Pascal; Université Clermont Auvergne, France

[5]Manufacture Française des Pneumatiques Michelin, Clermont-Ferrand, France


## Overview:

Multivariate time-series data contains valuable information but presents challenges for analysis and modeling. This project explores unsupervised representation learning approaches for extracting meaningful representations from unlabeled vehicle datasets. These representations help identify patterns in driving behavior and contribute to the prognosis and health management (PHM) of vehicle systems. Our primary objectives includes quantifying reliability and efficiency, measuring failure potential, reducing downtime, and improving component safety. We investigate various unsupervised feature extraction approaches, such as generative methods, change point detection, and encoder-only methods. Performance evaluation employs latent representations and their key performance indicators (KPIs) in tasks like clustering, classification, and regression. Actual multivariate car datasets spanning 2.5 years of driving data are employed, encompassing sensory information like accelerations, engine data, wheel speeds, and external temperature. By selecting the most suitable unsupervised methods and evaluating their effectiveness on these datasets, our objective is to enable their application in vehicle PHM tasks.

## Introduction

- Multivariate time series (MTS) are mostly **unlabeled**, **potentially long**, **irregular** and of **unequal lengths** in the same dataset
- Modeling MTS requires significant time and expertise
- Unsupervised representation extractions helps with:
  - Understanding **of underlying generating processes**
  - **Boosts performance of subsequent ML tasks**

- Objectives if this work:
  - Implement unsupervised representation extractions methods
  - Demonstrate strengths, weaknesses and suitability of application by evaluations via downstream tasks:
    - **Clustering**: grouping similar representations based on similarities or proximity
    - **Classification**: assigning labels or categories to representations
    - **Regression**: predicting other quantitative outputs using representations
    - **Anomaly detection**: identify rare or abnormal instances in representations
- Adequate performance on all downstream tasks, imply usability in PHM

## Vehicle use-case

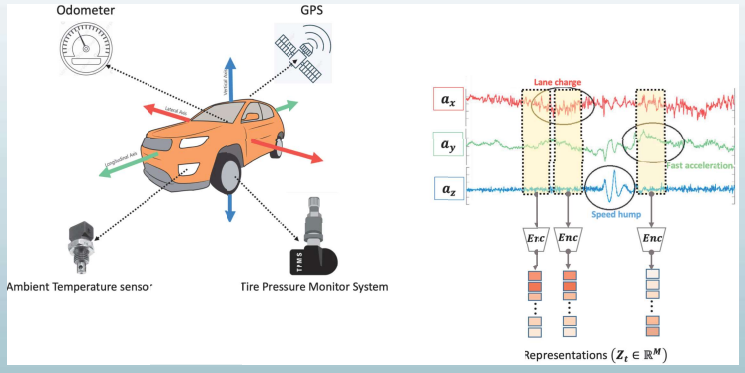


## Methods

- **Encoder-Decoder**: Generative modeling

$$X(W_t) = \boldsymbol{Enc}(W_t) \rightarrow Z \rightarrow \boldsymbol{Dec}(Z) = \bar{X}(W_t)$$

- **Change point detection (CPD)**: points where statistical properties change significantly

$$S(W_t) = \min_t(|\boldsymbol{Corr}(W_{t+1}) - \boldsymbol{Corr}(W_t)|)$$

- **Encoder-only**: unsupervised representation learning (knowledge extraction)

$$X(W_t) = \boldsymbol{Enc}(W_t) \rightarrow Z$$

Where:

- Encoder: $\boldsymbol{Enc}(\cdot)$, Decoder: $\boldsymbol{Dec}(\cdot)$ and a test statistic function: $S(W_t)$
- $X(W_t) \in \mathbb{R}^{F \times t}$, $F$: no. of features, $W_t$: temporal window at time $t$
- $Z \in \mathbb{R}^M$: some optimal low dimensional vector space
- $\boldsymbol{Corr}(\cdot)$ a correlation matrix

- These approaches employ sequential learning built on **Recurrent** or **Convolutional** Neural Networks


**Acknowledgements:** We would like to express our gratitude for the funding received from the European Union's Horizon 2020 research and innovation program, which was granted under the Marie Sklodowska Curie project **GREYDIENT** (Grant Agreement n° 955393). We would also like to acknowledge the ongoing support from Manufacture Française des Pneumatiques **Michelin** who provides us with the use-case car datasets.


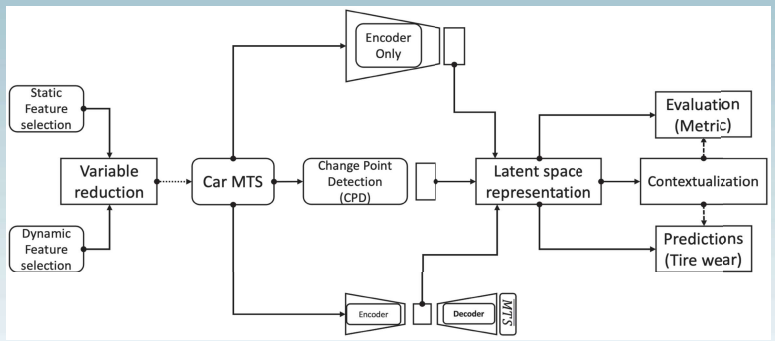


## Results

Use-case example:

- Encoder-only method applied on bivariate acceleration dataset
  - $Enc(\cdot)$ : is CNN with exponentially dilated convolutions
  - $T = 19273,\ W_t = 250,\ Z \in \mathbb{R}^{64}$

Accepted @IEEE PHM Conference (PHM2023), Paris

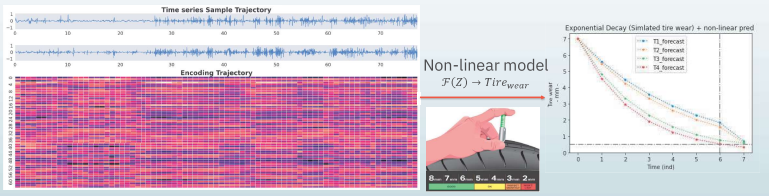


**Table: Evaluation on three downstream tasks: Clustering, Classification and Regression tasks**

| DATASET | Latent dimension | Model Training (Encoder-only: TNC) | | Clustering (K-means) | | | Cluster quality | | Classification (Linear classifier) | | Regression (Linear regression) | |
|---|---|---|---|---|---|---|---|---|---|---|---|---|
| | | Accuracy | Loss | Silhouette score | Davies Bouldin score | Calinski-Harabasz Index | Intra-Cluster Distance | Inter-Cluster Distance | AUPCR | Accuracy | Test: $R^2$ | MSE-Loss |
| 8 Days | $\mathbb{R}^{M=64}$ | 99.610 | 0.109 | 0.320 | 1.202 | 157099 | 0.516 | 0.884 | 0.976 | 84.470 | -0.288 | 1.255 |

## Industrial application

- Meaningful vehicle representations will be used for:
  - Monitoring daily **driving usage** and **anomalies**
  - Predict the **Remaining Useful Life (RUL)** of tires
  - Can be useful for **targeted tire design** and **manufacturing**

## Discussion

- Currently implemented **encoder-only** methods:
  - Generalized for all downstream tasks
  - Speedup for long time dependencies
  - **Hyperparameter optimization**: Latent dimensions, window-size and suitable architectures

- Ongoing work:
  - Make our **models large** (scale)
  - Evaluate on **long temporal vehicle data** with 2.5 years of driving
  - Incorporate different sensory data (considering irregularities)

## Bibliography


1. Representation with Triplet loss [J.Y. Franceschi, et.al. (2020)]
2. Representation Temporal Neighborhood Coding [S. Tonekaboni, et.al. (2021)]
3. Representation with Contrastive Predictive Coding [A. van den Oord, et.al. (2019)]
4. K-means: Classification and analysis of multivariate observations [J. MacQueen, (1967)]
5. t-SNE: Visualizing data using t-SNE [L. Van der Maaten, et.al. (2008)]
6. VAE: Variational Auto-Encoders [C.P. Burgess, et al. (2018)]
7. GP-VAE: Representation with Deep Probabilistic MVTS Imputation [V. Fortuin, et.al. (2020)]
8. DLG-VAE: Decoupled Local & Global Representation of MVTS [S. Tonekaboni, et.al. (2022)]
9. TiVaCPD: Time-Varying Correlation Nets for Interpretable Change Point Detection [K. Garg, et.al. (2022)]

# Maximum Entropy Probability Density Function from data

Guillaume Levillain[1], Pierre Beaurepaire[1] & Vincent Barra[2]

[1]Institut Pascal
[2]LIMOS

## Description of the problem

- When provided with samples obtained from a (random) data generation process, it is often difficult to find the probability density distribution that governs these points. The central limit theorem would tell us to expect a Gaussian repartition, but it would be only true if the data was truely random. Most of the time, the randomness comes from the stocasticity of the process.
- Facing this problem, there is no truely efficient methods to identify the PDF (Probability Density Function) of such data. State of the art methods tend to struggle to fit multimodal distributions.
- This work aims to resolve those limitations with the principle of maximum entropy, and unsupervised machine learning.
- The following example illustrates the task to solve:

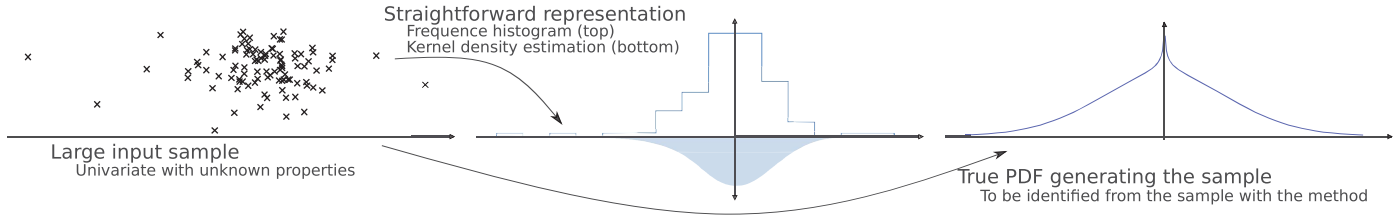


## Principle of Maximum Entropy

- This thesis aims then to identify a set $\{f_j\}_N$, and the optimal associated set $\{\lambda_j\}_N$ to fit at best a PDF on the prior data.
- The principle of maximum entropy states that the probability distribution maximizing the entropy, for some given prior data, is the most parsimonious.
- Maximizing the entropy is in a way equivalent to minimizing any preconceived assumption for the data distribution.
- Using this principle, the general shape of the PDF is given by:

$$p(x) = \exp\left(-\sum_{j=0}^{N} \lambda_j f_j(x)\right)$$

Where the $\lambda_j$ are Lagrange multipliers, $f_j$ the $n$ constrains function and with $f_0(x) = 1$ having $\lambda_0$ insuring that the PDF integrates to 1. The constrains functions are arbitrary choosen.

- This PDF form can seem strange, but we can find usual PDFs from it:
  - $\mathbb{E}[f_1(x)] = \mathbb{E}[x] = \frac{1}{\lambda},\ x \in \mathbb{R}^+ \rightarrow$ Exponential PDF
  - $\mathbb{E}[f_1(x)] = \mathbb{E}[x] = \mu,\ \mathbb{E}[f_2(x)] = \mathbb{E}\left[(x-\mu)^2\right] = \sigma^2,\ x \in \mathbb{R} \rightarrow$ Gaussian PDF

## Entropy of information

- To find relevant functions to describe the PDF, we search for those that are the best to "summarize" the data $\rightarrow$ Entropy-based metrics.
- The entropy, defined like $H[X] = -\int_\Omega p(x)\log_2(p(x))\,dx$, with $x \in \Omega$ (unit in bits). It represents the average quantity of information needed to describe the distribution.
- Entropy brings information on the probability density of a random variable, but we only have realisations of it.

## Neural Network constrains

- The maximum entropy PDF problem can be seen like a perceptron, with an exponential activation. The entropy of the estimated PDF, to be maximised, is given by :

$$H[X \mid f, \lambda] = \sum_{j=0}^{n} \lambda_j \mathbb{E}[f_j(x)]$$

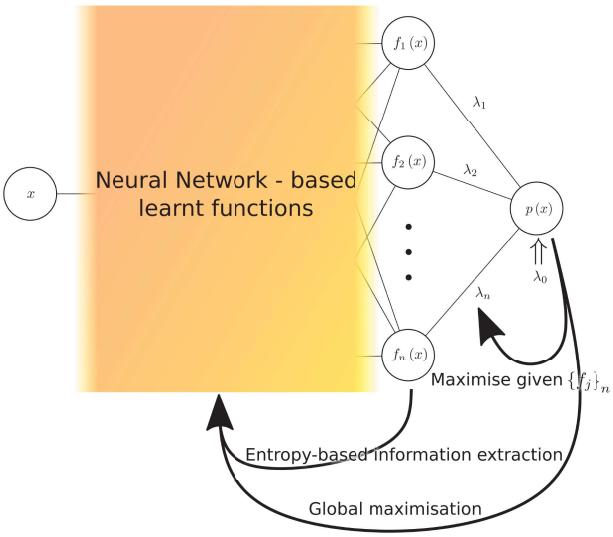


- The case of $\lambda_0$ is slightly peculiar. It has to be calculated from $\lambda_0 = \ln \int_\Omega \exp\left(-\sum_{j=1}^{n} \lambda_j f_j(x)\right) dx$. It can only be approximated.

## Conclusion

- Some work [1] already validates this approach using fractionnal moments functions ($f_j(x) = x^{\alpha_j},\ \alpha_j \in \mathbb{Q}$), but the results get rapidly worse when the shape of the PDF complexifies.
- First results with a very simple neural network and only the global maximization show very encouraging results. The optimisation of the $\{\lambda_j\}_n$ is trivial given the constrain functions, but there is no proof yet that this method shapes the constrains as we would want them to. Further work both analytical and experimental will be done to identify if the global optimization is sufficient or not for unusual PDFs.

## References

[1] P. L. Novi Inverardi and A. Tagliani.
Maximum entropy density estimation from fractional moments.

[2] Luis G. Crespo, Brendon K. Colbert, Sean P. Kenny, and Daniel P. Giesy.
On the quantification of aleatory and epistemic uncertainty using sliced-normal distributions.

[3] T.M. Cover and J.A. Thomas.
*Elements of Information Theory*.


guillaume.levillain@sigma-clermont.fr

# Suivi de consommation énergétique et d'ambiance pour la définition de stratégies de réhabilitation de sites commerciaux

## Cas d'étude : le parc immobilier de l'enseigne B&M (CIFRE)

**Françoise Misermont**
francoise.misermont@bmstores.fr
Directeur de thèse : Jean-Philippe COSTES (UCA-UMR Ressources),
Co-encadrant : Jean-Baptiste VIALE (UMR Ressources),
Partenaire CIFRE : Pascal LEPAILLER (B&M)

Ecole doctorale Sciences Pour l'Ingénieur

unité mixte de recherche ressources ensa CLERMONT-FERRAND

# Contexte

Le secteur du bâtiment représente 49% de la consommation d'énergie finale en France. La réduction de ces consommations au sein du secteur immobilier commercial est aujourd'hui une nécessité et répond à trois enjeux :

| Enjeux Environnementaux | Enjeux Economiques | Enjeux Réglementaires |
|---|---|---|
| Adaptation au changement climatique | Disponibilité et prix de l'énergie | Réduction des conso. de -60% d'ici 2050 |

# Problématique

L'atmosphère d'un point de vente influence ses usagers. Des dispositifs d'éclairage et de chauffage, adaptés à la stratégie commerciale, contribuent à la fabrication de cette atmosphère et représentent une part importante de la consommation d'énergie totale d'un établissement commercial. L'énergie est un facteur déterminant de l'expérience client et la réhabilitation énergétique un enjeu pour le commerce.

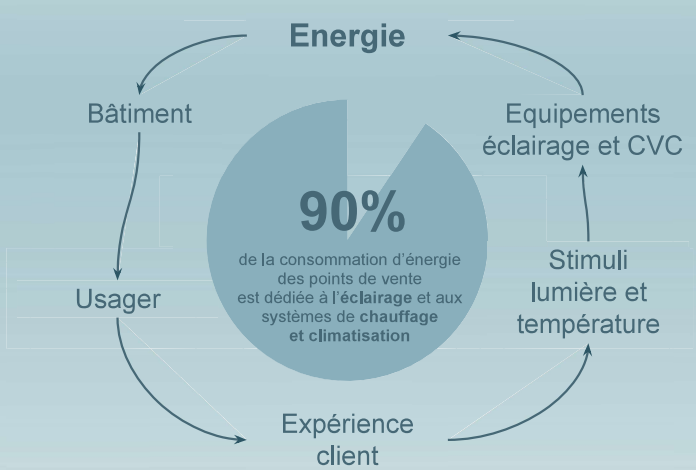


# Objectifs

1. Améliorer la connaissance du secteur tertiaire marchand et de ses enjeux face aux objectifs de baisse des consommations d'énergie
2. Analyser l'interdépendance entre objectifs commerciaux et réhabilitation énergétique pour une réussite commune et ses conséquence
3. Proposer une méthode aux entreprises de commerce qui souhaitent s'engager dans la réhabilitation énergétique de leur parc immobilier

# Données

Centre-ville | Centre-commercial | Commerce de périphérie

**110 ÉTABLISSEMENTS COMMERCIAUX ENSEIGNE B&M**
**-50% de consommation d'énergie entre 2011 et 2021**

| Techniques | | Sociales | Commerciales |
|---|---|---|---|
| Bâti | Consommations | | |
| . construction<br>. orientation<br>. zone climatique, … | 32 000 données/j (100%)<br>. Electricité (47%)<br>. Température (23%)<br>. Météo (22%)<br>. Eau (8%) | . Système de gérance et comportements énergétiques<br>. Responsabilité du bailleur et du preneur à bail | . Influence du stimuli lumière et température sur les comportements des usagers |

# Méthode

1. **Déterminer** le degré de maturité de l'enseigne : l'entreprise est-elle prête à inscrire durablement les enjeux environnementaux dans sa chaîne de valeur ?
2. **Définir** le panel d'études : quels sont les édifices concernés ?
3. Faire un **état des lieux**

| Energétiques | Stratégie commerciale |
|---|---|
| . sources de consommation d'énergie (équipements, pratiques, …), obsolescence des équipements, relation avec le bailleur | . Quelle est la stratégie commerciale actuelle ?<br>. Comment se traduit-elle en point de vente ? |

4. **Définir un cadre**, des attendus, des objectifs

| Energétiques | Stratégie commerciale |
|---|---|
| . Quelle est l'échelle de temps projetée ?<br>. Quels sont les objectifs ? | . Quelles sont les stratégies souhaitées ?<br>. Quelle atmosphère ? |

5. **Programmer** la stratégie à court, moyen et long terme.

# Bibliographie

1. Gwenaëlle Briand and Bernard Pras (2010) ,"Lighting and Perceived Temperature: Energy-Saving Levers to Improve Store Evaluations?", in NA - Advances in Consumer Research Volume 37, eds. Margaret C. Campbell, Jeff Inman, and Rik Pieters, Duluth, MN : Association for Consumer Research, Pages: 312-318 .
2. Kotler, P. (1974) "Atmospherics as a marketing tool". Journal of Retailing, 49, 48-64
3. Loureiro, Maria & Labandeira, Xavier (2019) "Exploring Energy Use in Retail Stores: A Field Experiment" Energy Economics, Elsevier, vol.84, https://doi.org/10.1016/j.eneco.2019.104570

# Multifunctional bioactive glass nanoparticles for bone tissue engineering

**Margot Muratet-Maraval**, Florestan Vergnaud, Charlotte Vichery, Jean-Marie Nedelec

*Université Clermont Auvergne, Clermont Auvergne INP, CNRS, ICCF, F-63000 Clermont-Ferrand, France*

Institut de Chimie de Clermont-Ferrand

## Introduction

### Background

**Multifunctional synthetic materials** are nowadays an **alternative to autografts and allografts** as raw resources for bone reconstruction, a necessary step after traumas or tumor resections leading to a significant bone loss.[1] If the bone loss induced is too important, natural bone regeneration is not sufficient and a bone graft must be performed. In this case, a surgical intervention is necessary, and bacterial infections can occur. This is why **the design of multifunctional materials**, combining **bone regeneration** and which could offer **antibacterial properties**, is sought.

### Objectives

The purpose of this work is to synthesize and study core-shell nanoparticles (NPs) based on **superparamagnetic iron oxide nanoparticles (SPIONs)** surrounded by a bioactive glass (BG) shell.

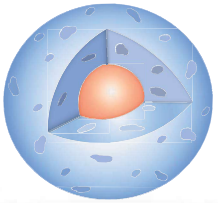

- Developed in the 1970s, **bioactive glasses** are well known to strongly bond *in vivo* with tissues, thanks to their dissolution mechanism, inducing **hydroxyapatite (HAp)** crystal formation at their surface and the liberation of ions promoting bone regrowth.[2] Here, the BG shell is **mesoporous**, in order to increase the material's exchange surface with biological fluids, and thus its bioactivity.[3]
- **Copper ions** are added to the glass composition to confer antibacterial properties and stimulate angiogenesis upon release after material implantation.[4]
- The **magnetic core ($\gamma$-$Fe_2O_3$)** can induce a local temperature increase through magnetic hyperthermia under **alternating magnetic field (AMF)**,[5] which could enhance ionic release. Also, the presence of SPIONs could promote osteoblast proliferation and differentiation.[6,7]

***Here, we studied the material bioactivity through HAp crystallization kinetics and copper release under different conditions.***

[1] Robert *et al.*, *Organogenesis*, 2012, 114 [2] Jones *et al.*, *Acta Biomater*, 2013, 9 [3] Misra *et al.*, *Biomaterials*, 2008, 1750 [4] Hoppe *et al.*, *Biomaterials*, 2011, 2757
[5] Wust *et al.*, *Lancet Oncol*, 3, 2002, 487 [6] Wang *et al.*, *J Mater Chem B*, 3, 2015, 4377 [7] Ota *et al.*, *PloS ONE* 12(7), 2017, 1

## Synthesis protocol

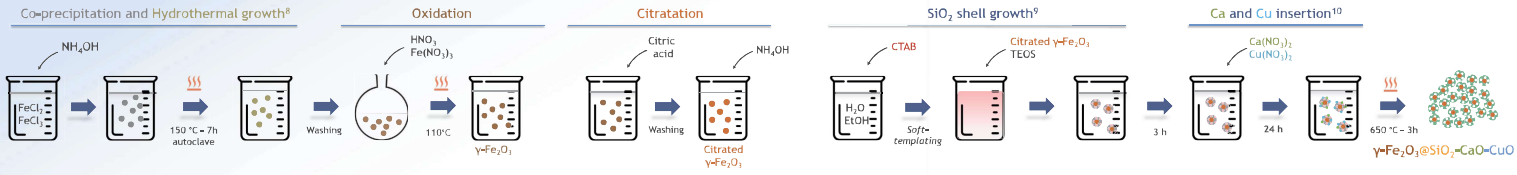


- ✓ **Magnetic cores** were synthesized by iron salts **coprecipitation** and a **glass shell** was grown using the **sol-gel** process (modified Stöber method)
- ✓ **Spherical** and **non-agglomerated** core-shell mesoporous nanoparticles were obtained

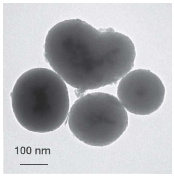


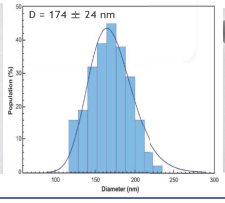


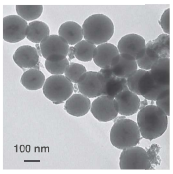


| Composition | $SiO_2$ | CaO | CuO | $Fe_2O_3$ |
|---|---|---|---|---|
| %wt | 64.6 ± 1.3 | 13.3 ± 1.3 | 11.9 ± 1.6 | 10.3 ± 1.9 |

| BET surface area ($m^2/g$) | BJH pore volume ($cm^3/g$) |
|---|---|
| 421.1 ± 11 | 0.343 ± 0.002 |

[8] Vichery *et al.*, *J. Phys. Chem. C*, 116, 2012, 16311
[9] Kesse *et al.*, *ACS Appl. Mat. Interfaces*, 12(42), 2020, 47820
[10] Vergnaud, *PhD thesis, Université de Clermont-Ferrand*, 2023

## Bioactivity

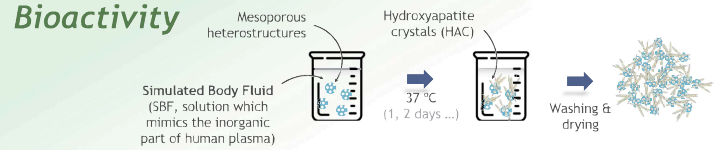


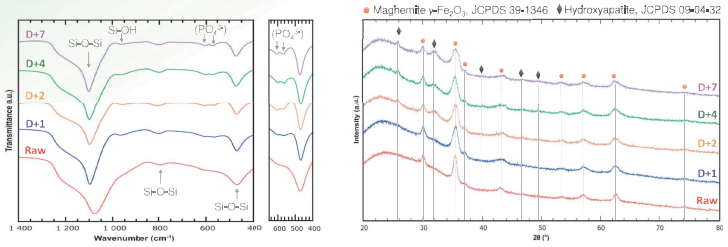


✓ **Hydroxyapatite formation** after immersion between **1 and 2 days** in SBF

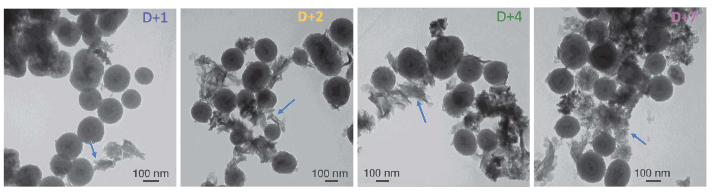


## Copper release in SBF

*Copper release after immersion in SBF at 37°C for different times (1 mg/mL)*

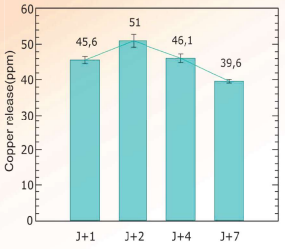


*Schematic mounting for copper release measurement (a) under AMF*

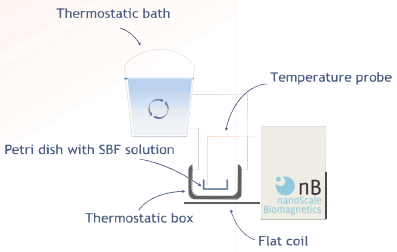


*Schematic mounting for magnetic colloids calorimetry experiments (SLP calculation)*

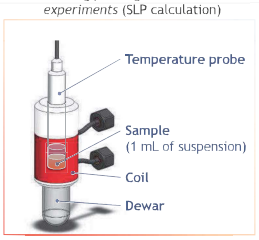


AMF Conditions : 768.15 kHz, 23.931 kA/m

↳ Specific Loss Power (SLP) = 184 $W/g_{Fe}$

*Copper release after immersion in SBF during 30 min for different temperature profiles (10 mg/mL)*

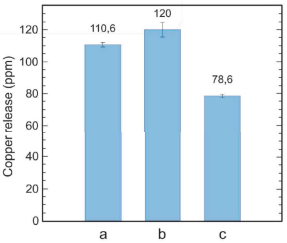


**a - Under AMF** (125.5 kHz, 31.83 kA/m)

**b - Temperature variation** (37 °C to 40 °C) similar to the one observed under AMF

**c - Fixed temperature** (37 °C)

- ✓ The **temperature** profile has an **effect** on **copper release** (enhanced when the temperature is increased).
- ✓ *After immersion in SBF* : **increase** in copper concentration until **day 2**, followed by a **decrease**. Could be explained by copper ions **adsorption** onto and/or **insertion** into newly formed **HAp** crystals.

## Conclusions & perspectives

- ➢ $\gamma$-$Fe_2O_3$@$SiO_2$-CaO-CuO : nanometric and non-agglomerated heterostructures were obtained. They have the ability to both promote bone tissue repair (fast hydroxyapatite formation) and induce copper release (enhanced by a temperature increase linked to magnetic stimulation).
- ➢ ***In vitro* assays** on osteoblastic cells will be carried out.
- ➢ Upcoming work will focus on shell **doping with new elements** of biological interest ($Zn^{2+}$, $Sr^{2+}$...).

# Experimental and numerical analysis of indoor contaminant dispersion and thermal comfort using particle tracking velocimetry

Mohammed MUSA[1], Pascal BIWOLE[1] ,Andre LABBE[2] ,Fabienne PENNEC[1]
[1]Université Clermont Auvergne, Institut Pascal UMR UCA/CNRS/SIGMA 6602
[2]Centre hospitalier universitaire CHU de Clermont-Ferrand
mohammed.musa@uca.fr

UNIVERSITÉ Clermont Auvergne
Ecole doctorale Sciences Pour l'Ingénieur

INSTITUT PASCAL

CLERMONT-FERRAND CENTRE HOSPITALIER UNIVERSITAIRE

## Problem

Globally, people spend about 90% of their time indoors (Fig 1(a)) and this has increased during COVID-19 lockdowns, with children spending more time indoors, enhancing potential indoor contaminants. Indoor air is indeed entrained with particles emitted by human breathing, activities, and indoor furniture (Fig 1(b)). it is important to be able to predict the trajectory and velocity of the air and airborne contaminants, in order to solve the challenge of poor indoor air quality and minimize building energy consumption required for a good indoor environment. Current optical methods such as Particle Image velocimetry (PIV) give only Instantaneous 2D vector field, and besides they can not be deployed to real habited rooms for safety reasons.

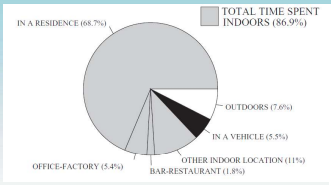


Fig 1(a)

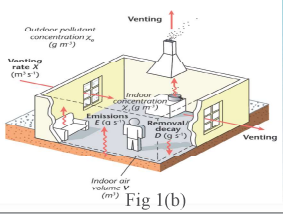


Fig 1(b)

## Objectives

- Development of a tool that can be used outside laboratories to measure, in real-time three-dimensional trajectory and the velocity of particles
- Application of the tool called 3DPTV (3D Particle Tracking Velocimetry) and Multi 3DPTV to study contaminant dispersion in rooms
- High-quality benchmark data set usable by air quality engineers and CFD communities
- Adapting 3DPTV to other areas of applications including optimization of inhaled therapy for children.

## Method

The 3D-PTV methodology uses synchronized photography from several calibrated camera locations (Fig 2a). To cover large measurement volumes we can further employ Multi-3DPTV, thanks to the stereo arrangement of cameras that allow intersections for multiple systems (Fig 2b)

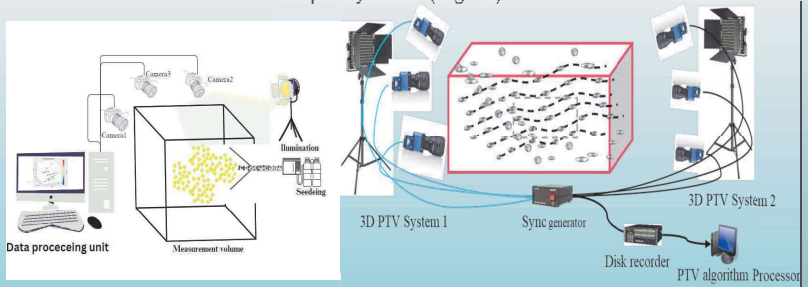


Figure 2: (a)A schematic sketch of a 3D-PTV(b) A schematic sketch of a Multi-3D-PTV

From such camera images, the 3D positions of the particles can be estimated using photogrammetry methods. Then, particle locations are linked in time to generate 3D trajectories that can be analyzed. Furthermore, time differentiation yields measurements of the particle's velocity and acceleration by the tracking algorithms (Fig 3)

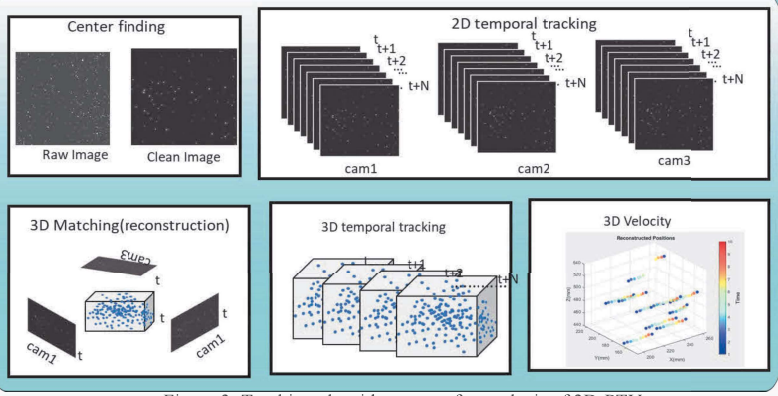


Figure 3: Tracking algorithms steps for analysis of 3D-PTV

## Results

**Validation:** Using a Synthetic sequence of images and random 3D positions the tracking algorithm accuracy was investigated visually

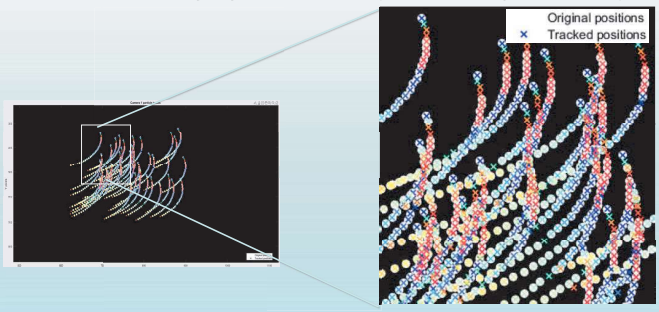


**Cough experiment:** The single 3DPTV system developed is used to track for 2 seconds at 60 fps (120 images) simulated single cough by a human manikin (exit velocity 21 m/s)

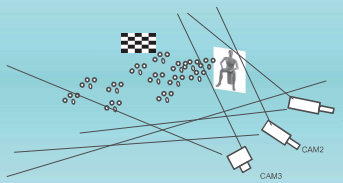


Figure 4: (a) Experimental setup (b) Schematic of Camera arrangement

### Single cough 2D temporal tracking results


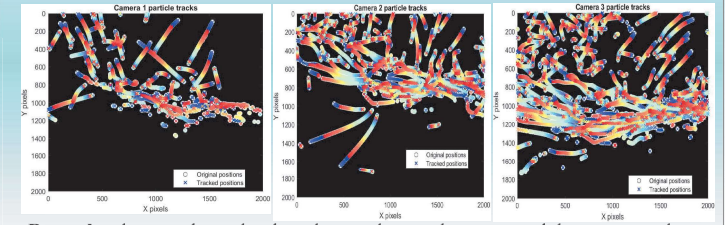


**Remarks**: there are large droplets close to the cough source, and the amount reduces across the camera arrangement further away from the source(right to left)

### Single cough 3D temporal tracking results

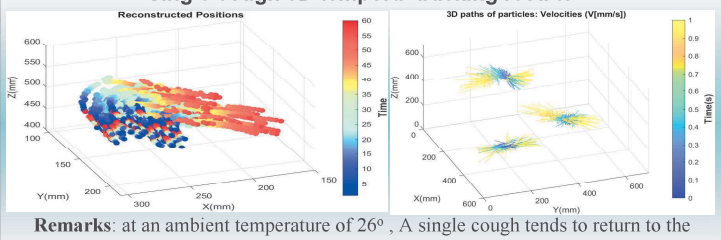


**Remarks**: at an ambient temperature of 26° , A single cough tends to return to the source in an enclosed room while velocity distribution remains relatively low

## Perspectives

1. Experiments in laboratory rooms using Multi 3DPTV to study contaminant dispersion in rooms and CFD validation
2. Real inhabited room experiment to provide recommendations
3. Application to a realistic transparent model of child airways to optimize inhale therapy

## Bibliography

[1] Biwole, P.H., Yan, W., Zhang, Y. and Roux, J.J., 2009. A complete 3D particle tracking algorithm and its applications to the indoor airflow study. Measurement Science and Technology.
[2] Janke, T. and Bauer, K., 2016. Development of a 3D-PTV algorithm for the investigation of characteristic flow structures in the upper human bronchial tree. In 18th International Symposium on the Application of Laser and Imaging Techniques to Fluid Mechanics, Lisbon, Portugal
[3] Fu, S., Biwole, P.H. and Mathis, C., 2015. Particle tracking velocimetry for indoor airflow field: A review. Building and Environment, 87, pp.34-44.

# Pickup and Delivery Problem with Cooperative Robots

**Chi Thao NGUYEN, Jean-Phillipe GAYON, Viet Hung NGUYEN**

*Laboratoire d'Informatique, de Modélisation et d'Optimisation des Systèmes*

Ecole doctorale Sciences Pour l'Ingénieur

## Introduction

- Warehouses are transferring from manual work to automatic.
- Deliver the package from a pickup point to a destination.
- Packages require more than one robot.
- Robots can reconfigure.
- Pickup and Delivery Problem with Cooperative Robots (PDP-CR).

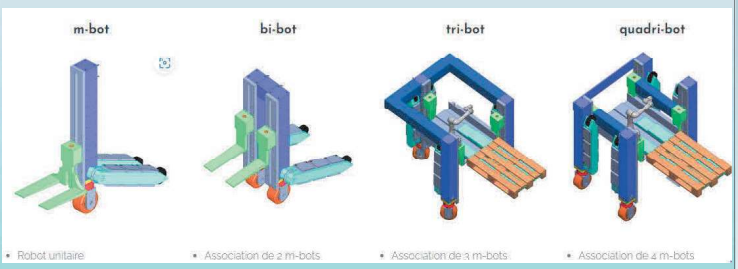


## Problem Definition

- Directed Graph $G = (V\ ,\ E\ )$.
- $R$ : number of robots.
- $T$ : number of tasks.
- Task $t$ requires $n_t$ robots, has pick-up location $p_t \in$ V and destination $d_t \in$ V.
- Robots must move synchronously to complete the task.
- Robot starts and ends its cycle at a depot.
- $c_{ij}$ : time for robot to move from node i to node j.
- Goal: minimize the sum of costs or makespan.

## Methods

MILP Models

### 1. VRP - Based

Expanded graph: expand task j with $n_j$ expanded tasks at the same location.

Every expanded task requires exactly one robot.

Synchronization between expanded tasks that have the same origin

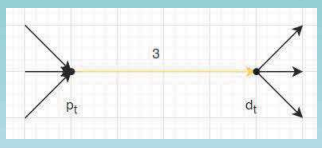


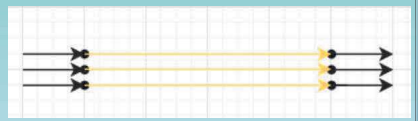

### 2. Flow – based

Every node can be visited multiple times.

Cannot straightforward find the waiting time.

## Results

Solved using CPLEX on lab's computer.

| total robots | total tasks | time | gap | num solved |
|---|---|---|---|---|
| 1 | 5 | 0.07 | 0.00 | 3 |
| 1 | 10 | 0.07 | 0.10 | 3 |
| 1 | 15 | 0.10 | 0.00 | 3 |
| 2 | 5 | 0.13 | 0.07 | 3 |
| 2 | 10 | 1.40 | 0.10 | 3 |
| 2 | 15 | 824.63 | 0.10 | 3 |
| 3 | 5 | 0.13 | 0.07 | 3 |
| 3 | 10 | 604.93 | 0.07 | 3 |
| 3 | 15 | 1905.30 | 0.40 | 1 |
| 4 | 5 | 0.10 | 0.10 | 3 |
| 4 | 10 | 11.50 | 0.10 | 3 |
| 4 | 15 | 1802.50 | 0.40 | 1 |

Table: Solve Result for VRP-based model with sum of costs objective

| total robots | total tasks | time | gap | num solved |
|---|---|---|---|---|
| 1 | 5 | 0.10 | 0.10 | 3 |
| 1 | 10 | 124.43 | 0.10 | 3 |
| 1 | 15 | 1802.47 | 0.80 | 3 |
| 2 | 5 | 0.13 | 0.10 | 3 |
| 2 | 10 | 1461.80 | 0.30 | 3 |
| 2 | 15 | 1801.27 | 0.83 | 3 |
| 3 | 5 | 0.20 | 0.10 | 3 |
| 3 | 10 | 1554.97 | 0.40 | 3 |
| 3 | 15 | 2134.60 | 0.90 | 3 |
| 4 | 5 | 0.20 | 0.10 | 3 |
| 4 | 10 | 1394.03 | 0.30 | 3 |
| 4 | 15 | 1846.53 | 0.90 | 3 |

Table: Solve Result for VRP-based model with makespan objective

| total robots | total tasks | time | gap | num solved |
|---|---|---|---|---|
| 1 | 5 | 0.10 | 0.03 | 3 |
| 1 | 10 | 149.40 | 0.10 | 3 |
| 1 | 15 | 1800.67 | 1.00 | 3 |
| 2 | 5 | 0.10 | 0.03 | 3 |
| 2 | 10 | 1680.20 | 0.57 | 3 |
| 2 | 15 | 1800.17 | 1.00 | 3 |
| 3 | 5 | 0.10 | 0.10 | 3 |
| 3 | 10 | 1446.73 | 0.43 | 3 |
| 3 | 15 | 1800.23 | 1.00 | 3 |
| 4 | 5 | 0.10 | 0.10 | 3 |
| 4 | 10 | 1215.20 | 0.30 | 3 |
| 4 | 15 | 1805.77 | 1.00 | 3 |

Table: Solve Result for flow-based model with makespan objective

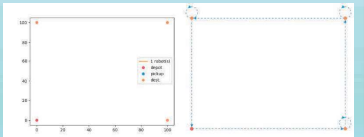

Figure: An example with 1 robot. the self-loop on the right figure denotes a robot going to a task 's destination,which is at the same location as its pickup node.

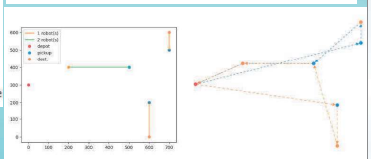

Figure: An example with 2 starting robots

## Conclusions

- Presented the Pickup and Delivery with Cooperative Robots Problem.
- Propose several MILP models.
- Solved using CPLEX, show numerical results.
- The problem size is still limited.

## Future Direction

- Applying heuristics.
- Make the constraints closer to real-life scenario: robots have battery and have to recharge after moving for some distance, the path is too narrow multiple robots cannot go through it...
- Multi-Agent Path Finding Problem (MAPF).
- Reinforcement Learning.

## Bibliography

"MecaBotiX." https://www.mecabotix.com/.

D. Bredström and M. Rönnqvist, "Combined vehicle routing and scheduling with temporal precedence and synchronization constraints," *European Journal of Operational Research*, vol. 191, pp. 19–31, Nov. 2008.

M. Drexl, "Synchronization in Vehicle Routing—A Survey of VRPs with Multiple Synchronization Constraints," *Transportation Science*, vol. 46, pp. 297–316, Aug. 2012.

G. Berbeglia, J.-F. Cordeau, and G. Laporte, "Dynamic pickup and delivery problems," *European Journal of Operational Research*, vol. 202, pp. 8–15, Apr. 2010.

S. N. Parragh, K. F. Doerner, and R. F. Hartl, "A survey on pickup and delivery problems: Part II: Transportation between pickup and delivery locations," *Journal für Betriebswirtschaft*, vol. 58, pp. 81–117, June 2008.

S. N. Parragh, K. F. Doerner, and R. F. Hartl, "A survey on pickup and delivery problems," *Journal für Betriebswirtschaft*, vol. 58, pp. 21–51, Apr. 2008.

B. L. Hollis, M. A. Forbes, and B. E. Douglas, "Vehicle routing and crew scheduling for metropolitan mail distribution at Australia Post," *European Journal of Operational Research*, vol. 173, pp. 133–150, Aug. 2006.

B. I. Kim, J. Koo, and J. Park, "The combined manpower vehicle routing problem for multi-staged services," *Expert Systems with Applications*, vol. 37, pp. 8424–8431, Dec. 2010.

# Star forest polytope for cactus graphs

NGUYEN Thanh Loan, NGUYEN Viet Hung

LIMOS, Université Clermont Auvergne

## Context

- In this thesis, we focus on the Maximum Weight spanning Star Forest Problem in graphs.
- The Spanning Star Forest
  - Given an undirected graph $G = (V, E)$ with a weight function $c : E \to \mathbb{R}_+$.
  - A *star* in $G$ is either an isolated node or a subgraph where all edges share a common endpoint.
  - A *star forest* refers to a collection of disjoint stars in $G$.

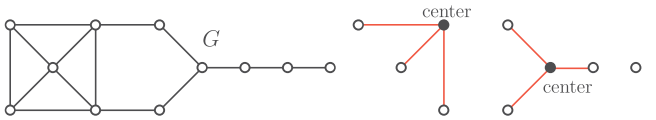


(a) An undirected graph $G$ (b) A star forest has 3 components in $G$.

  - A *spanning star forest* in $G$ is a star forest that spanning all vertex of $G$.
- The Maximum Weight spanning Star Forest Problem (MWSFP)
  - Input: A weighted graph $G = (V, E, c), c \in \mathbb{R}_+^{\mathbb{E}}$.
  - Output: A spanning star forest of $G$ with the largest size.
- The MWSFP is an NP-hard problem
  - The MWSFP can be reduced to the well-known minimum dominating set problem in the case of 0/1 weights [1].

## Applications

- In the aligning multiple genomic sequenced problems [1].
  - The threaded blockset aligner program utilizes a bottom-up approach to align multiple genomic sequences from various species based on the phylogenetic tree $T$. The comparison of phylogenetic trees involves the utilization of the spanning star forest problem.
  - For a specific internal node $v$ in $T$, let $B_v$ represent the blockset generated at that node. $v'$ and $v''$ are the left and right children of $v$, respectively. Considering a bipartite graph $G_v = (V', V'', E)$ in which:
    - The nodes in $V'$ and $V''$ are in a one-to-one correspondence with the blocks in $B_{v'}$ and $B_{v''}$, respectively.
    - Each edge $(x, y) \in E$ signifies that there exists a pairwise alignment $(a, b)$ such that $a$ and $b$ appear in the blocks associated with $x$ and $y$, respectively.

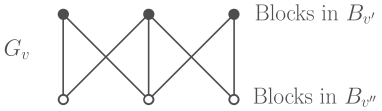


  In order to control the size of the output blockset, the maximum spanning star forest of $G_v$ is employed to merge the blocks $B_{v'}$ and $B_{v''}$.
- In the automotive industry. For instance, in the inclusion relation configurations digraph $DG = (V, A)$ in a car:
  - Each vertex represents a configuration and each arc $(u, v) \in A$ means that the configuration $v$ includes the configuration $u$.
  - $c_{uv}$ is the differential cost of the unit production costs of configuration $u$ and $v$.
  - The goal is to minimize the cost supply of produced configurations. It also means the objective is to determine a minimum arc cost sum of spanning star forests.

A spanning star forest with centers in $\{v_4, v_8\}$.

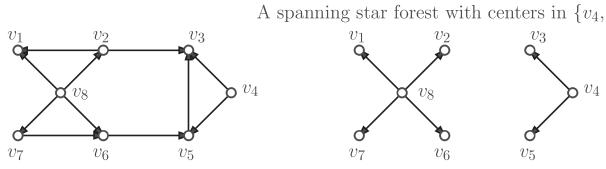


## Equivalence between $SFP(G)$ & MWSFP

- The Star Forest Polytope
  - A star forest polytope of $G$, denoted as $SFP(G)$, is the convex hull of the incidence vectors associated with the star forests in $G$.
- The MWSF problem of a graph $G$ can be formulated as an integer programming problem, where the objective function is $c^T x$, and the constraints precisely describe the polyhedron representing the star forests in $G$.

## Approaches

- Although there have been many studies on the MWSF problem, the investigation of its polyhedron has not been explored much. The work of Aider et al. [2] gave a complete description for $SFP(G)$ when $G$ is a tree or a cycle. Our purpose is to focus on *a polyhedral investigation of the MWSFP for cactus graphs*, a generalization of trees and cycles.
- A graph $G$ is a cactus graph if each edge of $G$ belongs to at most one cycle in $G$.

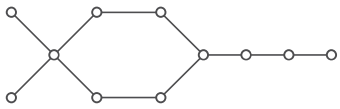

Figure: A cactus graph of order 11.

- Previous result for cactus graphs
  - In (Nguyen, [3]), Nguyen showed that the MWSF problem could be solved in linear time when $G$ is a cactus.

## Results

Our research demonstrates the characteristics of star forest polytope for cactus graphs.

- **Theorem.** When $G$ is a cactus graph and $\overrightarrow{G}$ is its associated bidirected graph. Then $SFP(G)$ is completely described by the following system.

$$x(E(C)) \leq \left\lfloor \frac{2|C|}{3} \right\rfloor, \forall \text{ cycle } C \subset G \quad (1)$$

$$x(\tau_{MV}) \leq |MV|, \forall \text{ MV-cactus } \tau_{MV} \subset G \quad (2)$$

$$x(E(C) \setminus P(C)) + 2x(P(C)) + x(\tau_{MVC}) \leq \frac{3|\hat{C}| + 3|\tilde{C}| - 1}{2} - |A'(C)| + |MVC|, \quad (3)$$

$$0 \leq x_e \leq 1, \forall e \in E. \quad (4)$$

$\forall$ g-odd cycle $C \subset \overrightarrow{G}$

## On going works

- This study allows us to consider if the star forest polytope can be separated in polynomial time for cactus graphs.
- As a part of the general case, this work can be used to improve the currently best ratio $\frac{1}{2}$ of the approximation algorithm ([1]) for the general case.

## References

[1] M. Hou L. Sheng W. Miller C.T. Nguyen, J. Shen and L. Zhang.
Approximating the spanning star forest problem and its applications to genomic sequence alignment.
*SIAM Journal on Computing*, 38(3):946–962, 2008.

[2] M. Baïou A. R. Mahjoub V. H. Nguyen M. Aïder, L. Aoudia.
On the star forest polytope for trees and cycles.
*Operations Research*, 53(5):1763–1773, 2019.

[3] V. H. Nguyen.
The maximum weight spanning star forest problem on cactus graphs.
*Discrete Mathematics, Algorithms and Applications*, 7(2):1550018, 2015.

[4] Sassano A. Vasilev .I Avella, P.
Computational study of large-scale p-median problems.
*Mathematical Programming*, pages 89—114, 2017.

[5] O. Cerdeira A. Agra, D. Cardoso and E. Rocha.
A spanning star forest model for the diversity problem in automobile industry.
*ECCO XVIII, Minsk, Belarus*, 2005.

[6] M. Baïou and F. Barahona.
The dominating set polytope via facility location.
*Combinatorial Optimization. ISCO 2014.*, 8596 of Lecture Note Computer Sciences:38—-49, 2014.

## Contact Information

- Email: thanh_loan.nguyen@uca.fr

# Nitrate removal from brackish groundwater via electrochemical process

OUTALEB, H.[1,2], GOURICH, B.[2], KOUZBOUR, S.[2], AUDONNET, F.[1], VIAL, C.[1]

[1]Université Clermont Auvergne, CNRS, Clermont Auvergne INP, Institut Pascal, Aubière, France.
[2]Laboratory of Process and Environmental Engineering, Higher School of Technology, Hassan II University of Casablanca, Morocco
Hamza.outaleb@doctorant.uca.fr

Ecole doctorale Sciences Pour l'Ingénieur

# Introduction

Brackish water comprises the largest portion of Earth's groundwater resources, particularly in semi-arid and arid regions, where elevated levels of chloride, potassium, sodium, magnesium, calcium, sulfate, bicarbonate and/or carbonate, culminating in the formation of a brackish groundwater (BGW) (1000 mg/L ≤ TDS ≤ 10,000 mg/L [1]. Furthermore, the use of nitrogen fertilizers and especially synthetic nitrate fertilizers or Urea-Urine-Fertilizer has resulted in an elevated concentration of nitrate in BGW due to its high solubility in water, allowing for easy leaching through soils and subsequent entry into groundwater [2]. Nitrate contamination cause acute health problems to newborns (methemoglobinemia "baby-blue syndrome") [3]. Several conventional techniques such as adsorption, ion exchange, reverse osmosis, chemical, and biological processes have been developed for the nitrate removal. However, these techniques have several limitations such as requirement of post-treatment, less efficiency, and high installation costs [4].
Interest in electrochemical processes, like electrocoagulation (EC) and electrochemical nitrate reduction (eNO3RR), has been continuously growing. This techniques are considered today as one of the most promising technologies for effectively remove nitrate from groundwater. The primary objective of this study was to examine the significance of the cathode material as a critical parameter in the process of nitrate reduction from BGW. The investigation aimed to investigate the role of different cathode materials and optimize their properties, with the goal of utilizing copper foam (Cu foam) as a cathode material in future studies to further enhance the nitrate reduction process. By comparing various cathode materials, the study aimed to lay the foundation for the future implementation of Cu foam as a highly efficient cathode material in nitrate removal by EC from BGW.

# Methods

Experiments were carried out in an undivided electrolytic cell of volume 0.25 L (and working volume of 0.2 L) in batch mode with two parallel electrodes of anode (Aluminum) and cathode (Aluminum, Iron and Copper) arranged vertically and with dimensions of 10 cm × 5 cm × 0.1 cm, and IKA C-MAG MS 7 Magnetic Stirrer. All the experiments were carried out for a magnetic stirring of 200 rpm. Electrodes were connected to a digital DC supply (VOLTCRAFT DSP-3005V) in the galvanostatic mode with voltage range of 0-30 V and current intensity range of 0-5 A. For all experiments, the room temperature was 20±1°C. Before each experiment, the electrodes were abraded with sandpaper to clear the scales, soaked in 1N $H_2SO_4$, rinsed with ultrapure water (18.1 MΩ.$cm^{-1}$) to remove impurities, and then immersed in treated water for 10 min before being in the EC cell. A picture of the experimental setup is depicted in **Fig. 1**. The main chemical and physical properties of the synthetic BGW are presented **in Table 1**. Fixed and Operating parameters and cell design are summarized in **Table 2**.

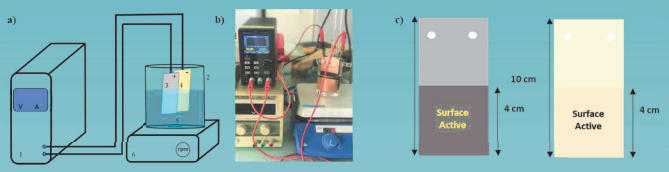


**Fig. 1.** **(a)** schematic sketch of electrochemical cell used for nitrate removal, 1: DC power supply; 2: electrolytic cell; 3: anode plate; 4: cathode plate; 5: magnetic bar-stirrer 6: magnetic stirrer. **(b)** Experimental setup for nitrate removal, **(c)** schematic diagram of electrodes plate.

**Table 1** Physicochemical characteristics of the artificial brackish groundwaters used in the experiments.

| Parameters | Artificial brackish groundwater |
|---|---|
| pH | 8.1 |
| Conductivity (mS/cm) | 11.58 |
| Calcium $Ca^{2+}$(mg/L) | 557 |
| Potassium $K^{+}$(mg/L) | 7.8 |
| Sodium $Na^{+}$(mg/L) | 447 |
| Magnesium $Mg^{2+}$(mg/L) | 315 |
| Chlorides $Cl^{-}$(mg/L) | 1250 |
| Sulfates $SO_4^{2-}$(mg/L) | 416 |
| Bicarbonates $HCO_3^{-}$(mg/L) | 290 |
| Nitrates $NO_3^{-}$ (mg/L) | 100 |

**Table 2** Abridgement of operating parameters and cell design.

| Parameters | Values / units |
|---|---|
| anode | Aluminum Al |
| cathode | Aluminum Al |
| | Iron Fe |
| | Copper Cu |
| Inflow pH | 8.1 |
| Current density | [15, 20, 25, 30 mA/cm²] |
| Chloride concentration | [0.3, 0.4, 0.5, 0.6 A] |
| Initial $NO_3^{-}$ concentration | [100 mg/L] |
| Electrolysis time | [180 min] |
| Reactional volume | 0,2 L |
| Interelectrode distance | [1 cm] |
| Active anodic area | 20 cm² |

# Results

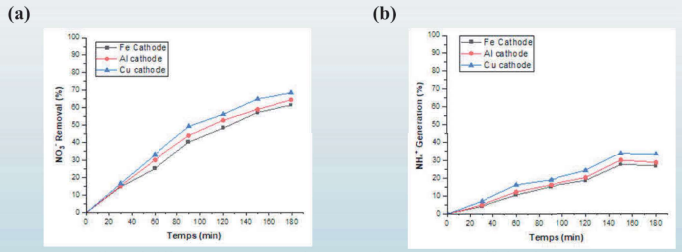


**Fig. 1.** The effect of different cathode material on **(a)** nitrate removal efficiencies and **(b)** ammonium formation. ($[NO_3^-]_i$= 100 mg/L, pH=8.1)

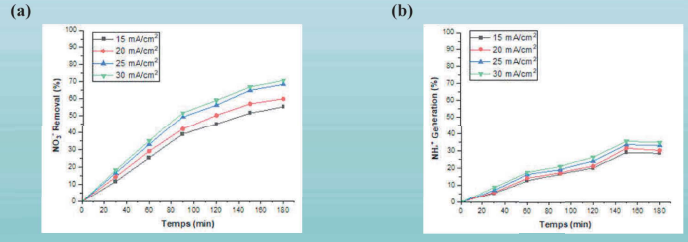


**Fig. 2.** The effect of current density on **(a)** nitrate removal efficiencies and **(b)** ammonium formation. ($[NO_3^-]_i$= 100 mg/L and pH=8.1)

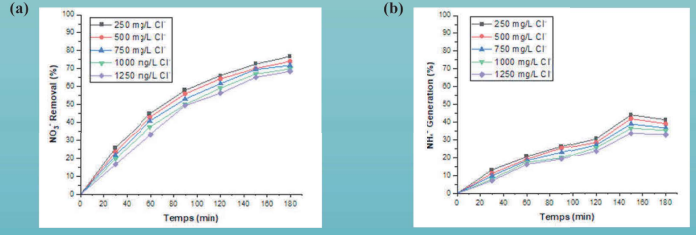


**Fig. 3.** The effect of chloride ions on **(a)** nitrate removal efficiencies and **(b)** ammonium formation. ($[NO_3^-]_i$= 100 mg/L, j=25 mA $cm^{-2}$)

In this study three different materials, aluminum (Al), iron (Fe) and Copper (Cu) were examined as cathode and aluminum was used as an anode. As depicted in **Fig. 1**, the cathodic electrode plays a significant role in the process of nitrate removal by EC. The percentage removal of $NO_3^-$ was higher for the copper electrode (68.55%) compared to both tested electrodes (Al and Fe), which exhibited comparable removal rates of 64.55% and 61.54%, respectively. Among the various current densities examined, the one at 30 mA $cm^{-2}$ demonstrated the highest efficiency in residual nitrate removal. After 180 minutes of treatment time, it achieved an approximate nitrate removal of 71%, surpassing the removal efficiencies observed at other tested current densities (**Fig. 2**). Due to the high concentration of chloride in BGW, we investigated its influence on nitrate removal. **Fig.3** showed that higher chloride concentrations led to a decrease in nitrate removal efficiency. Conversely, lower concentrations of chloride were associated with higher ammonium formation.

# Conclusions

In conclusion, the cathode material is considered a key factor of EC performance, because it affects nitrate reduction and ammonium formation during the process. Furthermore, higher current density increased the nitrate removal efficiency. furthermore, the higher chloride concentration decreased the nitrate reduction. The findings of this study indicate that enhancing the cathode can be achieved by incorporating a 3D electrode, such as Cu foam, to increase the active surface area. Additionally, the study suggests that optimizing various operating parameters, including current density, pH, and applied voltage, can have a crucial impact on improving the overall process.

# Bibliography

[1] Y.D. Ahdab, G.P. Thiel, J.K. Böhlke, J. Stanton, J.H. Lienhard, Minimum energy requirements for desalination of brackish groundwater in the United States with comparison to international datasets, Water Research. 141 (2018) 387–404. https://doi.org/10.1016/j.watres.2018.04.015.

[2] T. Biswas, S.C. Pal, I. Chowdhuri, D. Ruidas, A. Saha, A.R.Md.T. Islam, M. Shit, Effects of elevated arsenic and nitrate concentrations on groundwater resources in deltaic region of Sundarban Ramsar site, Indo-Bangladesh region, Marine Pollution Bulletin. 188 (2023) 114618. https://doi.org/10.1016/j.marpolbul.2023.114618.

[3] F.R. Greer, Infant Methemoglobinemia: The Role of Dietary Nitrate in Food and Water, PEDIATRICS. 116 (2005) 784–786. https://doi.org/10.1542/peds.2005-1497.

[4] S. Tyagi, D. Rawtani, N. Khatri, M. Tharmavaram, Strategies for Nitrate removal from aqueous environment using Nanotechnology: A Review, Journal of Water Process Engineering. 21 (2018) 84–95. https://doi.org/10.1016/j.jwpe.2017.12.005.

# Accostage Haute Précision d'un chariot autonome à fourche - Accrobot

Julien Pascal[1], Paul Checchin[1], Benoit Thuilot[1]

[1]Universite Clermont Auvergne, Clermont Auvergne INP, CNRS, Institut Pascal, F-63000 Clermont-Ferrand, France

Ecole doctorale Sciences Pour l'Ingénieur

La Région Auvergne-Rhône-Alpes

## Problématique adressée

AGV déplaçant des bobines

- **Objectif** : Automatiser le transport de charges dans des ateliers existants
- **Contraintes** : sols non parfaitement plats, allées étroites, scènes encombrées, environnement dynamique, positionnement imprécis des charges lourdes, environnement non communicant

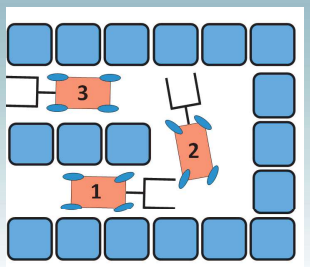


Plus grande agilité

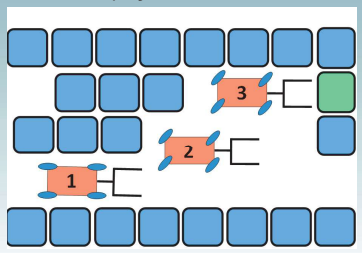


Marche en crabe

- Configuration de **véhicule avec deux trains de direction indépendants :** offre la possibilité de négocier des **virages très serrés** et de se **déplacer en crabe**
- Cependant, le fait qu'une **fourche** prolonge le véhicule complique considérablement les algorithmes de contrôle automatique.

**Quelle trajectoire** pour un véhicule à deux trains directeurs **encombré d'une fourche à l'avant ?**

## Planification de trajectoire

- Variante du **Fast Marching** [1], introduite dans [2] et adaptée ici pour ce type de véhicule, avec ses contraintes spécifiques

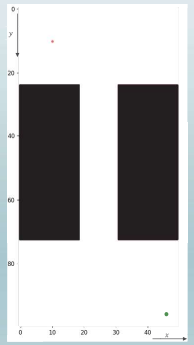

Modélisation de l'environnement dans une grille binaire

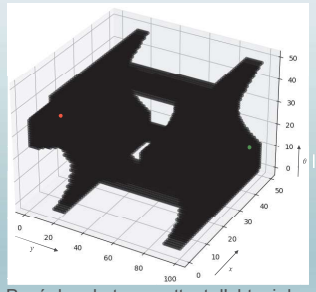

Posé de robot permettant d'obtenir les triplets $(x, y, \theta$ = orientation) qui ne donnent pas lieu à une collision

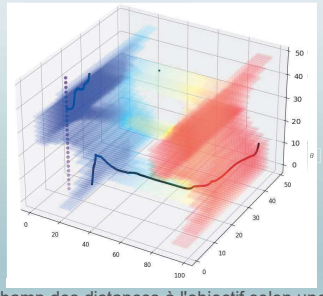

Champ des distances à l'objectif selon une métrique adaptée à ces véhicules + trajectoire optimale dans l'espace $(x, y, \theta)$

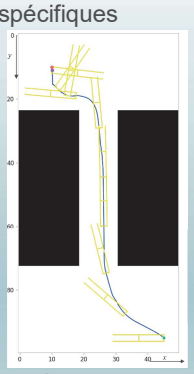

Trajectoire finale obtenue par descente de gradient

| | Reeds-Shepp[3] | Euler-Mumford elastica[4] | Dubins[5] |
|---|---|---|---|
| Coût en fonction de :<br>• $\kappa$ la courbure<br>• $\xi$ un paramètre assimilable à un rayon de courbure | $C^{RS}(\kappa) = \sqrt{1 + \lvert\xi.\kappa\rvert}$ | $C^{EM}(\kappa) = 1 + \lvert\xi.\kappa\rvert^2$ | $C^{D}(\kappa) = \begin{cases} 1 \; si \; \lvert\xi.\kappa\rvert < 1 \\ \infty \; sinon \end{cases}$ |
| Métrique pour $p = (x, \theta), x \in \mathbb{R}^2$ $n(\theta) = (\cos(\theta), \sin(\theta))$ | $F_p(\dot{p}) = \begin{cases} \lVert\dot{x}\rVert * C\left(\frac{\lvert\dot{\theta}\rvert}{\lVert\dot{x}\rVert}\right) \; si \; \dot{x} = \lVert\dot{x}\rVert n(\theta) \\ \infty \; sinon \end{cases}$ | | |

Métrique de distance intégrant les contraintes cinématiques du véhicule

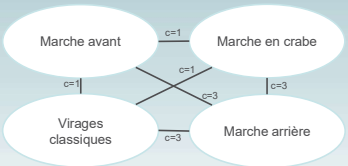


Mécanisme d'états avec des coûts de transition pour favoriser les comportements privilégiés

Utilisation de la **géométrie hamiltonienne** pour obtenir un chemin optimal, favorisant les mouvements privilégiés, qui intègre nativement toutes les contraintes de ces robots agiles

## Résultats et Performances

| | |
|---|---|
| Posé de robot | 1s |
| Calcul de la fonction de potentiel + descente de gradient | 1,04 s |

- Espace $(x, y, \theta)$ de 100x100x100
- Tests effectués sur un processeur Intel Core i7-11850 à 2,5GHz*16 et un GPU Nvidia T1200

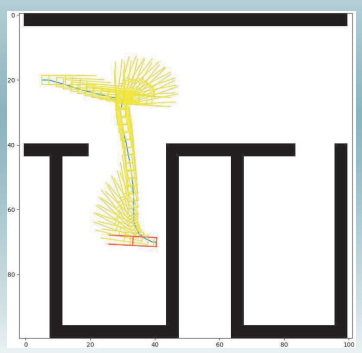

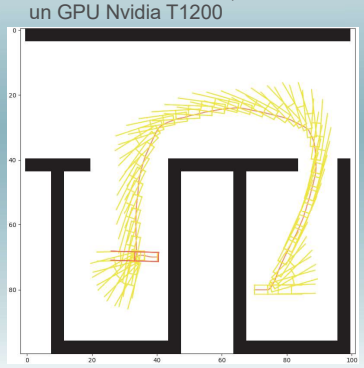

Exemples de trajectoires générées par notre méthode

## Conclusion

- **Toute l'agilité** du robot prise en compte et trajectoire **directement utilisable sans besoin d'étapes supplémentaires**
- Des **préférences utilisateur** peuvent être introduites dans le calcul de la trajectoire
- **Replanification en-ligne** possible
- **Expérimentation** avec robot Adap2e à venir

## Bibliographie

[1] J. A. Sethian, "A fast marching level set method for monotonically advancing fronts." Proceedings of the National Academy of Sciences, vol. 93, no. 4, pp. 1591–1595, 1996.

[2] J.-M. Mirebeau, "Fast Marching methods for Curvature Penalized Shortest Paths," Journal of Mathematical Imaging and Vision, vol. 60, no. 6, pp. 784–815, 2018. [Online]. Available: https://hal.science/hal-01538482

[3] J A Reeds and L A Shepp. Optimal paths for a car that goes both forwards and backwards. Pacific Journal of Mathematics, 145(2):367 393, 1990.

[4] L Euler. Methodus inveniendi Lineas curvas maximi minive proprietate gaudentes. Lausanne/Geneva: Bousquet, 1744

[5] L E Dubins. On curves of minimal length with a constraint on average curvature, and with prescribed initial and terminal positions and tangents. American Journal of Mathematics, 79:497–516, 1957

# Heterogeneous Camera Heterogeneous Netwok Simulator


Ecole doctorale Sciences Pour l'Ingénieur

**Romain POUILLARD**
*Institut Pascal*


## Context

SmartCamera:
- High resolution
- High-performance processus

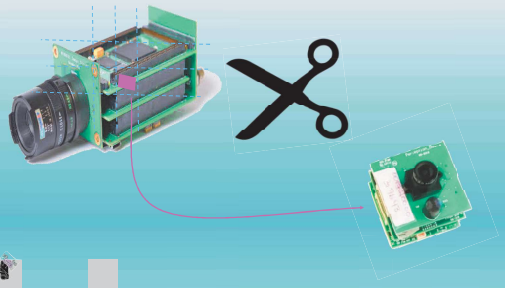

SillyCam:
- Low Resolution
- Low performance
- Wireless

- Smart Camera

- Silly Camera Network

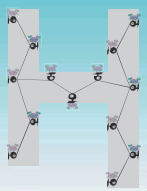

## RoadMap

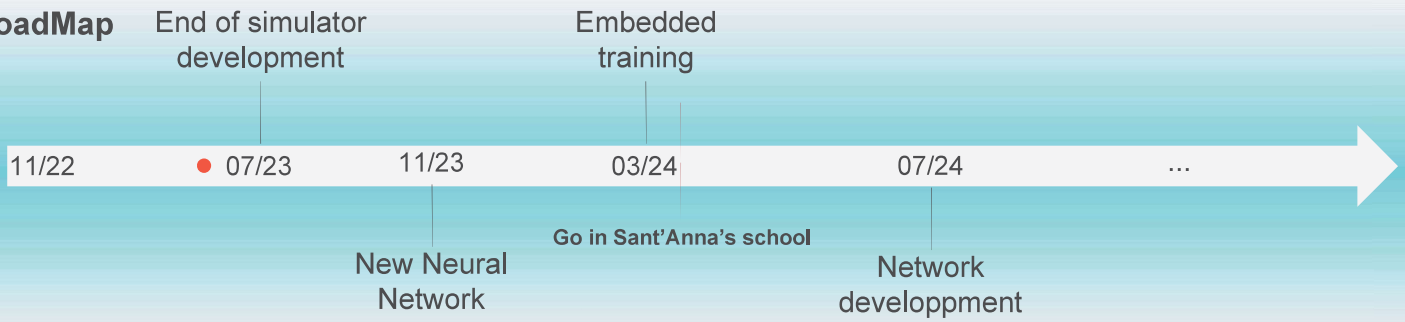


## Simulator

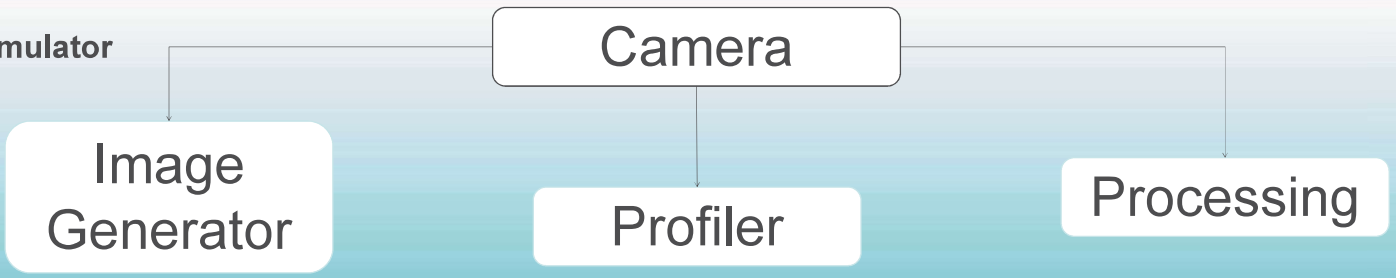


- Build environment
- Create a scenario
- Generate image render

- Ressources
  - Hardware
  - Memory
- Consumption

- 3 Types of processing:
  - FPGA
  - CPU
  - GPU
- Each instance have CPU process to schedule and network managing

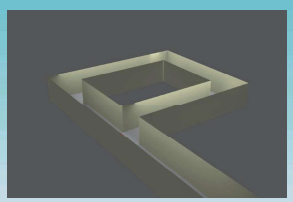

Example of environment

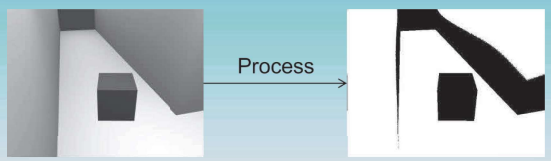


Example of processing FPGA

# Senologic Surgery With Augmented Reality

R.SHARIFIAN[1,2], S.MADADZADE[3], W.MARRAOUI[4], A.BARTOLI[1,2]

1. Institut Pascal, UMR6602 CNRS, Clermont-Ferrand University Hospital
2. SurgAR, Surgical Augmented Reality, Clermont-Ferrand
3. Service de sénologie et imagerie du sein, centre Jean-Perrin, Clermont-Ferrand
4. Service de chirurgie oncologique, centre Jean-Perrin, Clermont-Ferrand

Ecole doctorale Sciences Pour l'Ingénieur

## Introduction

**Preoperative localisation of the cancerous breast lesions involves Wire Guided Localisation. WGL, is done by placing a fine thread-like wire close to the cancerous region [1]. Even if inserting the guidance objects inside the breast is performed under local anaesthesia, it can be painful and is often very traumatic [2]. We propose an non-invasive Augmented Reality substitution pipeline for tumour localisation.**

Breast tumour localization using mammograms and with metal clips. The objective in this PhD is to propose a replacement method by augmented reality.

## Methods

### Breast tumour Augmented Reality steps

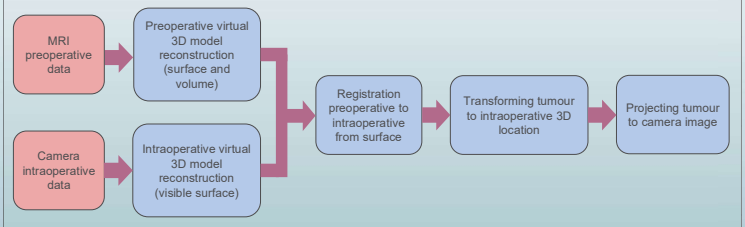


### MRI in supine position with board on breast

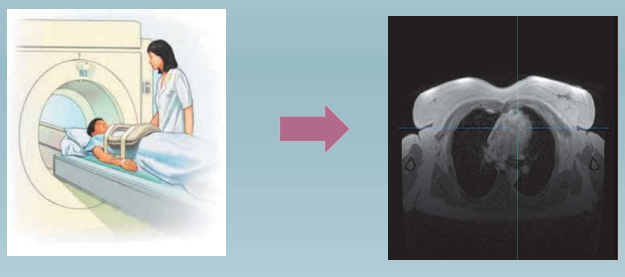

### Reconstructing Virtual 3D Preoperative Models

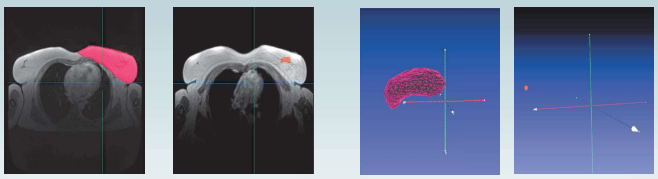

Breast segmentation | Tumour segmentation | Breast 3D model | Tumour 3D model

### Intra-operative data acquisition and 3D model reconstruction

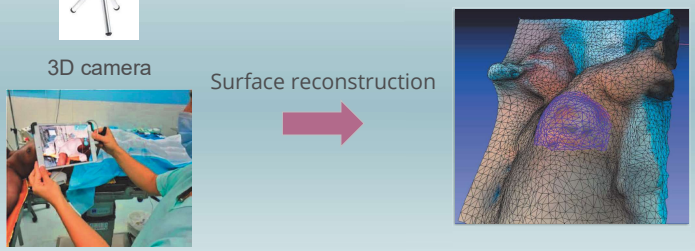


Operating room data acquisition

Patient's intraoperative model (breast in purple)

## Results

### Registration

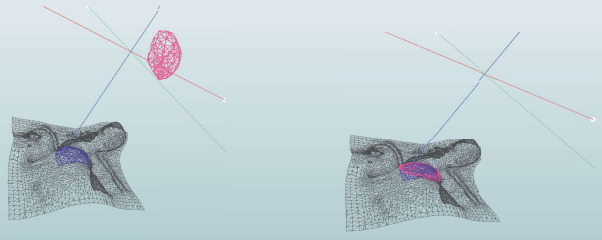

Preoperative model (purple) and intraoperative model (pink) before registration: we see that they are **not at the same spatial location**

Registering preoperative model to intraoperative model **Done manually with Meshlab**

### Breast surface and tumour augmentation

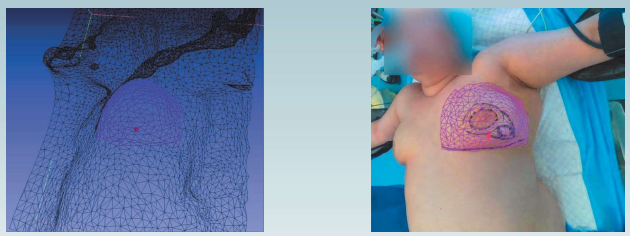

Transforming the tumour (red mesh) to appropriate position based on the calculated registration

Generating the augmented image by projecting the tumour and breast models to camera plane

## Bibliography

1. *Postma. "Efficacy of 'radioguided occult lesion localisation'(ROLL) versus 'wire-guided localisation'(WGL) in breast conserving surgery for non-palpable breast cancer: a randomised controlled multicentre trial." Breast cancer research and treatment, vol. 136, 2012, 469--478.*

2. *Postma. "Localization of nonpalpable breast lesions." Expert review of anticancer therapy, vol. 11, 2011, 1295 --1302.*

# DEGRADATION OF ORGANIC POLLUTANTS FROM PHARMACEUTICAL WASTEWATER IN ALGERIA USING LOCAL GREEN MICROALGAE


**BOCHRA SOUMATI[1,2,3] , ADHYA-EDDINE HAMITOUCHE[2], CHRISTOPHE VIAL[1], ALINA-VIOLETA URSU[1*], DAVID DUCHEZ, CHRISTINE GARDARIN[1], ABD-ELMOUNEÏM BELHADJ[3]**

[1]UNIVERSITÉ CLERMONT AUVERGNE, CLERMONT AUVERGNE INP, INSTITUT PASCAL, CLERMONT-FERRAND, FRANCE
[2]CENTER FOR SCIENTIFIC AND TECHNICAL RESEARCH IN PHYSICOCHEMICAL ANALYSIS, TIPAZA, ALGERIA
[3]LABORATORY OF BIOMATERIALS AND TRANSPORT PHENOMENA, UNIVERSITY OF MÉDÉA, 26000, MÉDÉA, ALGERIA



## Abstract:

The aim of the present study was to provide an integrated view of the algal removal of diclofenac (DCF). A microalgae strain isolated Chlorella sp. was cultured under different concentrations of DCF and their growth, chlorophyll production and diclofenac removal efficiency were monitored. The results showed that DCF had strong effects on microlagae growth after 5 days. The microalgae showed DCF removal efficiency. The amounts of removed DCF in presence of Chlorella sp were up to 36.71%, 79.94%, 77.83%,90.20%, and 83.33% of 9, 14, 20, 50 and 80 mg L−1, respectively. This study indicated that Coelastrella thermophila had good growth capacity and DCF removal efficiency and could therefore be used for the treatment of aqueous systems contaminated with DCF.


## Introduction

Emerging contaminants are a myriad of trace organic compounds including prescription and over-the-counter pharmaceuticals, veterinary, personnel care products like cosmetics, sunscreens and fragrances [1]. One of the biggest contributors of pharmaceuticals and personal care products (PPCPs) in the environment are wastewater treatment plants (WWTPs) [2]. The removal of some pharmaceuticals in conventional wastewater treatment plants is rather low due to their high solubility and low biodegradability [3]. Among the most used PPCPs, Diclofenac (DCF) is a non-steroidal anti-inflammatory drug (NSAID) widely prescribed as an antipyretic analgesic
Therefore, it is mandatory to investigate alternative treatments for DCF removal from wastewaters. Among them, those based on the use of microalgae are emerging as a sustainable and economical solution [4].

## Materials and methods

- the DCF which is a Solution for injection at 75 mg/3mL.
- *Coelastrella thermophila* was isolated from a lake "Bir Ben Osmane" located in East of Algeria.

**Preliminary tests:**
-Growth of microalgae in different concentration of DCF.

**Culture conditions:**
-Different concentration of DCF:
0, 9, 14, 20, 50, 80 mg/L in culture media (TAP)
-Agitation at 135 rpm
Illumination (24/24 h lighte cycle) of 75 µmol/ m². s-1

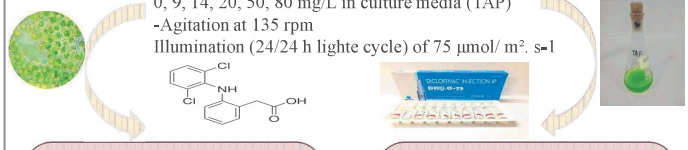

**Evaluation of microalgae growth:**
-measuring the optical density of the algal culture at 600 and 750 nm by spectrophotometer
-Chlorophyll extraction

**Determination of residual DCF in the medium:**
-HPLC analysis

**DCF removal (%)** $= \frac{(initial - final)\ concentration\ of\ DCF}{initial\ concentration\ of\ DCF}$

## Preliminary Results

**1-Effect of DCF on microalgae growth:**

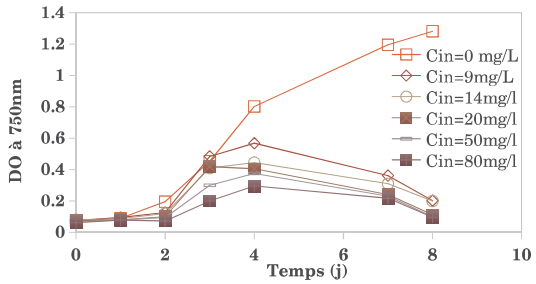


Fig-1- Growth of *Coelastrella thermophila* in different concentration of DFC in TAP media at 750 nm

the presence of diclofenac in the TAP medium negatively influences the growth of the microalgae, which means the toxicity of DCF on the growth of the microalgae

**2-Impact of DCF on production of chloropyll (a+b):**

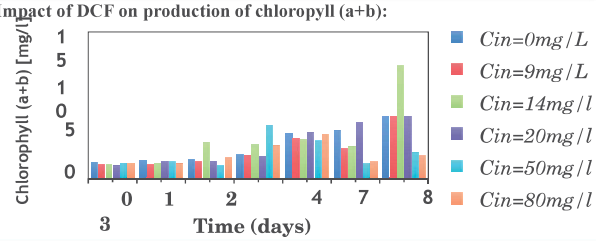


the chlorophyll content in Coelastrella themophila decreased steadily with increasing diclofenac concentration. which concluded that the antibiotic DCF was toxic for Coelastrella thermophila.

**3-DCF removal from the culture medium :**

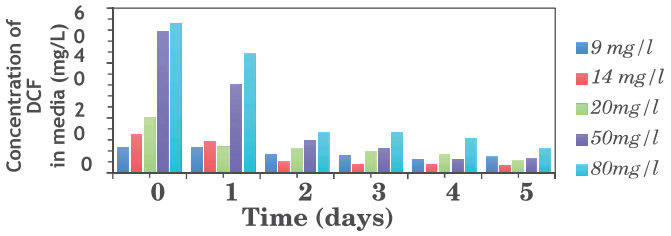


The DCF removal by Coelastrella thermophila at 9, 14, 20, 50 and 80 mg L−1 DCF after 5 days of treatment .
The best DCF removal yield 90.20% for an initial concentration of 50 mg/L.

## Conclusion and perspectives

Cell growth and chlorophyll (a+b) production of microalgae decreased with increasing of DCF concentration
Microalgae can eliminate the presence of a high concentration of DCF but only in the residual medium and this is what encouraged us for the following perspectives:
-study of the mechanism of DCF degradation by microalgae
Monitoring of the influence of the presence of DCF in the culture medium on the (bio)chemical composition of the microalgal biomass: soluble proteins (photocolorimetric assay), fatty acids (GC/MS)


**Acknowledgments:**

this work is part of the PHC Tassili project (2021-2023) between France and Algeria (CMEP 46093SJ)



**References:**

1. Field,J.A . et al. (2006), Environ. Sci. Technol. 40, 7105.
2. Blair B. et al. (2015), Chemosphere, 134, 395–401.
3. Escapa C. et al. (2018), Sci. Total Environ. 640–641.

# Problèmes de conception de réseaux et d'optimisation de tournées autour de la mise en place de circuits courts alimentaires de proximité

Arnauld Tuyaba[1], Laurent Deroussi[1], Nathalie Grangeon[1], Sylvie Norre[1], Sophie Rodier[2]

Université Clermont Auvergne, INP, UMR 6158 LIMOS[1], EA 3849 CleRMa[2], France

## Contexte et objectifs de la thèse

- Mise en place de la loi EGAlim dans la restauration collective.
- Objectif: proposition et optimisation d'organisations logistiques satisfaisant les demandes de la restauration collective.
- Collaboration avec la Chambre d'Agriculture de l'Allier et le Conseil Départemental de l'Allier.

## Conception des réseaux de distribution

Circuits courts alimentaires de proximité: au plus un intermédiaire et 80 km.

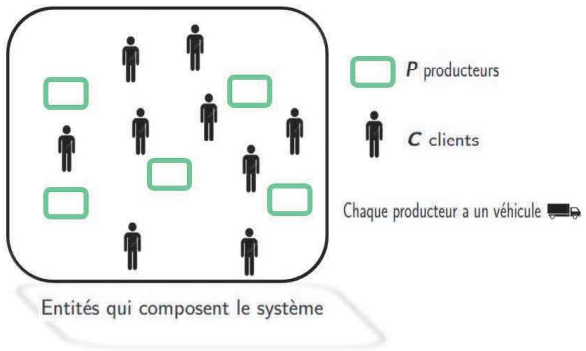


Trois scénarios sont envisagés:

- Scénario 1: chaque producteur livre ses clients de façon indépendante

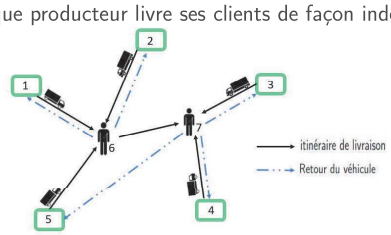


Scénario 1

- Scénario 2: les producteurs mutualisent leurs tournées

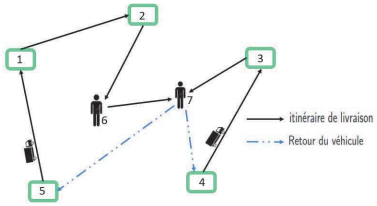


Scénario 2

Dans ce cas nous avons distingué deux versions:

- version 1: les clients passent les commandes auprès d'une plateforme
- version 2: les clients passent les commandes directement aux producteurs

- Scénario 3: Dépôts intermédiaires permettent de regrouper les produits avant redistributions aux clients:
  - nombre et dimensionnement des dépôts
  - mutualisation ou non des tournées

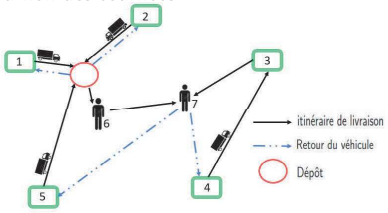


Scénario 3

## Formulation mathématique

### Données

- $P, C, N = P + C$
- $D_{i,j}$ matrice des distances
- $Q^n_{c,p}$ demande du produit $n$ du client $c$ auprès du producteur $p$
- $C_p$ ensembles des clients du producteur $p$
- $V$ ensembles des véhicules des producteurs
- $Cap_p$ capacité de véhicule du producteur $p$

### Scénario 1

- Variables de décision
  - $X_{i,j} = 1$ si le véhicule passe par l'arc $(i, j)$ et $0$ sinon
  - $f_{i,j}$ : nombre d'unités transportées par le véhicule sur l'arc $(i, j)$
- Objectif

$$\min \sum_i \sum_j D_{i,j} \times X_{i,j}$$

- Contraintes
  - livraison en une seule fois pour chaque client
  - satisfaction des demandes des clients par produit
  - respect de la capacité du véhicule

### Scénarios 2 et 3

- Variables de décision
  - $X^k_{i,j} = 1$ si le véhicule $k$ passe par l'arc $(i, j)$ et $0$ sinon
  - $qp^k_{c,p}$ : quantité chargée par le véhicule $k$ du client $c$ chez le producteur $p$
  - $qc^k_{c,p}$ : quantité livrée par le véhicule $k$ chez le client $c$ venant du producteur $p$
  - $q^k_i$: quantité de produit dans le véhicule $k$ lorsqu'il quitte le noeud $i$
  - $y^k_i$: variable auxiliaire
- Objectif

$$\min \sum_k \sum_i \sum_j D_{i,j} \times X^k_{i,j}$$

- Contraintes
  - satisfaction des demandes des clients par produit
  - respect des capacités de production et des véhicules
  - élimination des sous-tours.

## Instance et Résultats

### Exemple d'instance

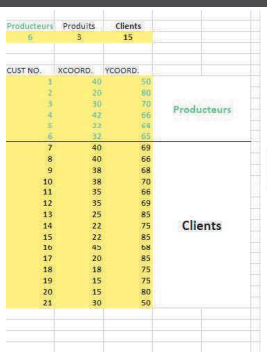


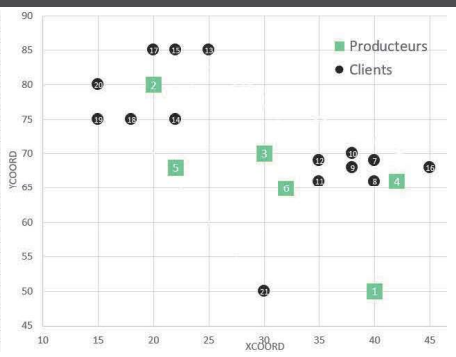


### Résultats

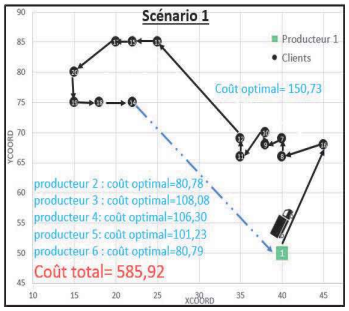


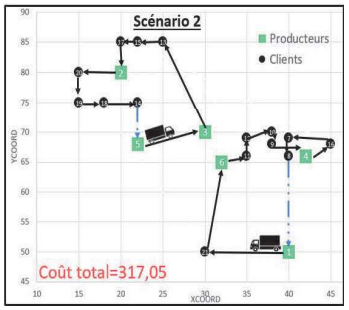




arnauld.tuyaba@doctorant.uca.fr